Voltage and Ca^{2+} Activation of Single Large-Conductance Ca^{2+}-activated K^+ Channels Described by a Two-Tiered Allosteric Gating Mechanism✪

Brad S. Rothberg and Karl L. Magleby

From the Department of Physiology and Biophysics, University of Miami School of Medicine, Miami, Florida 33101-6430

abstract The voltage- and Ca^{2+}-dependent gating mechanism of large-conductance Ca^{2+}-activated K^+ (BK) channels from cultured rat skeletal muscle was studied using single-channel analysis. Channel open probability (P_o) increased with depolarization, as determined by limiting slope measurements (11 mV per e-fold change in P_o; effective gating charge, q_{eff}, of 2.3 ± 0.6 e_o). Estimates of q_{eff} were little changed for intracellular Ca^{2+} (Ca^{2+}_i) ranging from 0.0003 to 1,024 μM. Increasing Ca^{2+}_i from 0.03 to 1,024 μM shifted the voltage for half maximal activation ($V_{1/2}$) 175 mV in the hyperpolarizing direction. $V_{1/2}$ was independent of Ca^{2+}_i for $Ca^{2+}_i \leq 0.03$ μM, indicating that the channel can be activated in the absence of Ca^{2+}_i. Open and closed dwell-time distributions for data obtained at different Ca^{2+}_i and voltage, but at the same P_o, were different, indicating that the major action of voltage is not through concentrating Ca^{2+} at the binding sites. The voltage dependence of P_o arose from a decrease in the mean closing rate with depolarization ($q_{eff} = -0.5$ e_o) and an increase in the mean opening rate ($q_{eff} = 1.8$ e_o), consistent with voltage-dependent steps in both the activation and deactivation pathways. A 50-state two-tiered model with separate voltage- and Ca^{2+}-dependent steps was consistent with the major features of the voltage and Ca^{2+} dependence of the single-channel kinetics over wide ranges of Ca^{2+}_i (~0 through 1,024 μM), voltage (+80 to −80 mV), and P_o (10^{-4} to 0.96). In the model, the voltage dependence of the gating arises mainly from voltage-dependent transitions between closed (C-C) and open (O-O) states, with less voltage dependence for transitions between open and closed states (C-O), and with no voltage dependence for Ca^{2+}-binding and unbinding. The two-tiered model can serve as a working hypothesis for the Ca^{2+}- and voltage-dependent gating of the BK channel.

key words: large-conductance Ca^{2+}-activated K^+ channel • K_{Ca} channel • Monod-Wyman-Changeux • Eigen • Markov

INTRODUCTION

Large conductance Ca^{2+}-activated K^+ channels (BK or maxi K^+ channels)[1] are activated by both intracellular calcium (Ca^{2+}_i) and depolarization of the membrane potential (Marty, 1981; Pallotta et al., 1981; Barrett et al., 1982; Latorre et al. 1982; Methfessel and Boheim, 1982; Wong et al., 1982). Once open, BK channels allow the passive flux of K^+ out of cells, driving the membrane potential more negative. This reduction of membrane excitability by active BK channels plays a key role in the function of a wide variety of tissues by linking intracellular Ca^{2+}_i to membrane potential, in which the tightness of the linkage is increased by depolarization (reviewed by Latorre, 1994; Conley, 1996; Kaczorowski et al., 1996; Toro et al., 1998).

Some of the structural regions contributing to the voltage and Ca^{2+} sensitivity of BK channels have been identified. The pore-forming alpha subunits of BK channels, which are encoded by the gene at the *Slo* locus (Atkinson et al., 1991; Adelman et al., 1992; Butler et al., 1993; Tseng-Crank et al., 1994), assemble as tetramers to form functional channels (Shen et al., 1994). The alpha subunits show homology with the pore-forming subunits of the voltage-dependent superfamily of K^+ channels, including an S4 voltage sensor (Atkinson et al., 1991; Butler et al., 1993; Jan and Jan, 1997; Diaz et al., 1998), gating charge movement with voltage activation (Stefani et al., 1997; Horrigan and Aldrich, 1999), and voltage-dependent gating in the virtual absence of Ca^{2+}_i, (Pallotta, 1985; Meera et al., 1996; Rothberg and Magleby, 1996; Cui et al., 1997; Horrigan et al., 1999; Nimigean and Magleby, 2000; Talukder and Aldrich, 2000). The COOH terminus of BK channels is much longer than that of other K^+ channels, exceeding the length of the core region, and contains the primary Ca^{2+}-sensing domain of the channel (Wei et al., 1994; Schreiber and Salkoff, 1997; Schreiber et al., 1999).

Dr. Rothberg's present address is Department of Neurobiology, Harvard Medical School, Boston, MA 02115.

Portions of this work were previously published in abstract form (Rothberg, B.S., and K.L. Magleby. 1996. *Soc. Neurosci. Abstr.* 22:1443. Rothberg, B.S., and K.L. Magleby. 1999. *Biophys. J.* 76:A333. Rothberg, B.S., and K.L. Magleby. 2000. *Biophys. J.* 78:92A).

Address correspondence to Dr. Brad S. Rothberg, Department of Neurobiology, Harvard Medical School, 220 Longwood Ave., Boston, MA 02115. Fax: 617-734-7557; E-mail: brothberg@hms.harvard.edu; or Dr. Karl L. Magleby, Department of Physiology and Biophysics, P.O. Box 016430, Miami, FL 33101-6430. Fax: 305-243-6898; E-mail: kmagleby@miami.edu

✪The online version of this article contains supplemental material.

[1]*Abbreviations used in this paper:* BK channel, large conductance calcium-activated K^+ channel; MWC, Monod-Wyman-Changeux; NLR_1, normalized likelihood ratio per interval pair.

Gating mechanisms proposed to account for the Ca^{2+} and/or voltage sensitivity of BK channels have typically been based on the 10-state Monod-Wyman-Changeux model (MWC; Monod et al., 1965; Changeux and Edelstein, 1998) or the 35-state Eigen model (Eigen, 1968; see scheme one in Cui et al., 1997). Both of these models describe conformational changes for a tetrameric allosteric protein. The separate movement of the four subunits in the Eigen model compared with the joint (concerted) movement in the MWC model leads to the much larger numbers of states in the Eigen model. These models, as well as the Koshland-Nemethy-Filmer sequential model, which represents a subset of states in the Eigen model, are discussed in Fersht (1985). While both the MWC and Eigen models or modifications of these models can give excellent descriptions of the channel kinetics over restricted ranges of conditions (Magleby and Pallotta, 1983; McManus and Magleby, 1991; Wu et al., 1995; Cox et al., 1997; Cui et al., 1997; Rothberg and Magleby, 1998; Horrigan et al., 1999; Horrigan and Aldrich, 1999), both models with Ca^{2+}_i as the allosteric activator fail to describe the data at the extreme conditions of either ~0 Ca^{2+}_i (Horrigan et al., 1999; Nimigean and Magleby, 2000; Talukder and Aldrich, 2000) or saturating (1 mM) Ca^{2+}_i (Rothberg and Magleby, 1999).

To overcome these limitations, we have extended the MWC and Eigen models to two-tiered gating mechanisms comprised of at least 50 states in their minimal theoretical form, with 25 closed states on the upper tier and 25 open states on the lower tier (Rothberg and Magleby, 1999). Such two-tiered models with Ca^{2+}_i as the allosteric activator can account for the Ca^{2+} dependence of the gating for a fixed voltage from low to saturating levels of Ca^{2+}_i, including predicting the Hill coefficients for Ca^{2+} activation and the correlation between adjacent open and closed intervals (Rothberg and Magleby, 1999). Alternatively, a two-tiered model with voltage as the allosteric activator can account for the voltage dependence of the gating at ~0 Ca^{2+}_i (Horrigan et al., 1999; Horrigan and Aldrich, 1999). Thus, two-tiered models can account for the Ca^{2+} dependence of the gating at a fixed voltage and for the voltage dependence of the gating at ~0 Ca^{2+}. It will now be crucial to test whether two-tiered gating mechanisms can also describe the complex interactions between Ca^{2+}_i and voltage (see commentary by Jones, 1999).

The purpose of the present study is to evaluate the ability of a two-tiered allosteric gating mechanism to describe both the Ca^{2+} and voltage-dependent activation of BK channels. Using single-channel recording techniques, we examine the effects of voltage on the open and closed interval durations over wide ranges of Ca^{2+}_i. The resulting dwell-time distributions and estimates of P_o are analyzed to examine the relationship between activation by Ca^{2+}_i and voltage and estimate the charge movement associated with the voltage-dependent activation and deactivation of the channel. We find that two-tiered models provide a reasonable description of the Ca^{2+}_i and voltage dependence of the gating from ~0 to saturating levels of Ca^{2+}_i over wide ranges of voltage and P_o. In terms of the two-tiered mechanism, the voltage dependence of the gating arises mainly from voltage-dependent transitions between the closed (C-C) and open (O-O) states, with less voltage dependence for transitions between the closed and open states (C-O), and with no voltage dependence of the Ca^{2+}-binding and -unbinding steps. Ca^{2+}_i modulates the voltage for half activation, while having little effect on the effective gating charge for activation. These findings on the voltage-dependent steps obtained with single-channel analysis over a range of voltage and Ca^{2+}_i are consistent with those obtained from macroscopic ionic and gating currents at ~0 Ca^{2+}_i (Horrigan et al., 1999; Horrigan and Aldrich, 1999).

The two-tiered model provides a comprehensive gating mechanism for BK channels that can simultaneously describe the major features of the steady state activation by both Ca^{2+}_i and voltage over wide ranges Ca^{2+}_i, voltage, and P_o.

METHODS

Preparation and Single-Channel Recording

Currents flowing through single BK channels in patches of surface membrane excised from primary cultures of rat skeletal muscle (myotubes) were recorded using the patch-clamp technique (Hamill et al., 1981). Cultures of rat myotubes were prepared from fetal skeletal muscle as described previously (Barrett et al., 1982; Bello and Magleby, 1998). All recordings were made using the excised inside-out configuration of the patch-clamp technique in which the intracellular surface of the patch was exposed to the bathing solution. Unless otherwise indicated, analysis was restricted to patches containing a single BK channel. Experiments were performed at room temperature (22–24°C).

Solutions

The solutions bathing both sides of the membrane contained 150 mM KCl and 5 mM TES [*N*-tris(hydroxymethyl)methyl-2-aminoethane sulfonate] pH buffer, with the pH of the solutions adjusted to 7.0. Contaminant Ca^{2+}_i was determined by atomic absorption spectrometry. Ca^{2+} (as $CaCl_2$) was added to bring the Ca^{2+} concentration at the intracellular surface (Ca^{2+}_i) to the indicated levels. The solutions did not contain Ca^{2+} buffers unless indicated. Very low Ca^{2+}_i of ~0.0003 and ~0.03 μM was obtained by adding 2 mM EGTA and 0 or 266 μM Ca^{2+}, respectively, to the solution. No Ca^{2+} was added to the extracellular (pipette) solution. Solutions were changed through the use of a microchamber (Barrett et al., 1982).

Analysis Restricted to Activity in the Normal Mode

All data analyzed in this paper were restricted to activity in the normal mode, which typically includes ~96% of the intervals (McManus and Magleby, 1988). Unless otherwise indicated, the analysis was performed using the same methods presented in detail in earlier papers (Rothberg and Magleby, 1998, 1999). Briefly,

single-channel currents were recorded on a digital data recorder (DC-37 kHz), low-pass filtered with a four-pole Bessel filter to give a final effective filtering of 6–10 kHz (−3 dB), and sampled by computer at a rate of 125–200 kHz. The filtering gave effective dead times (Colquhoun and Sigworth, 1995) for the following channels (μs): 16 B04, 17.9 B14, 22.9 B12, and 28.5 B06, B07, B10, B13, B15, and B16. The methods used to set the level of filtering to exclude false events that could arise from noise, measure interval durations with half-amplitude threshold analysis, test for stability, and identify activity in the normal mode using stability plots, are as described previously (McManus et al., 1987; McManus and Magleby, 1988, 1989; Magleby, 1992). The use of single channel analysis to study gating of BK channels allows secondary effects of Ca^{2+}, such as Ca^{2+}-dependent mode shifts to the low activity mode (Rothberg et al., 1996) to be clearly identified and excluded from the analysis of normal mode activity.

Estimates of P_o were obtained by dividing the observed open time by the sum of the observed open and closed times. Although missed events can have large effects on estimates of interval durations, they had negligible effect (<1%) on the estimates of P_o. The reason for this is that, under the conditions of our experiments, the intervals that were missed were very brief compared with the mean durations of the intervals that were captured, so that missed events removed a negligible amount of the total time.

Estimating Rate Constants and Evaluating Kinetic Models

Estimates of the most likely rate constants, including their Ca^{2+} and voltage sensitivities, were made from the simultaneous (global) fitting of two-dimensional dwell-time distributions obtained at several different Ca^{2+}_i and voltages, using Q-matrix methods (Colquhoun and Hawkes, 1995b) incorporating the Crouzy and Sigworth (1990) correction for missed events (details in Rothberg and Magleby, 1998, 1999). Such fitting of 2-D distributions takes into account the correlation information in the single-channel data (Fredkin et al., 1985; Magleby and Weiss, 1990; Magleby and Song, 1992). Microscopic reversibility was preserved during the fitting to be consistent with the gating of BK channels (Song and Magleby, 1994).

Normalized likelihood ratios (NLR_1) were used to indicate how well any given kinetic scheme describes the 2-D dwell-time distributions when compared with a theoretical best description of the data (Rothberg and Magleby, 1998, 1999). Normalization corrects for differences in number of interval pairs among experiments, allowing direct comparisons between different experiments. The normalized likelihood ratio per interval pair is defined as Eq. 1:

$$NLR_1 = \exp[(\ln S - \ln T)/n], \quad (1)$$

where ln$S$ is the natural logarithm of the maximum likelihood estimate for the observed 2-D dwell-time distributions given the kinetic scheme, ln$T$ is the natural logarithm of the likelihood of the theoretical best description of the observed distributions, and n is the total number of fitted interval pairs (events) in the observed dwell-time distributions (McManus and Magleby, 1991; Rothberg and Magleby, 1998). For comparison to data normalized to 1,000 interval pairs, as also used in our previous studies, NLR_{1000} is given by $NLR_1{}^{1000}$.

The NLR_1 gives a measure of how well different kinetic schemes describe the distributions, but it cannot be used to directly rank schemes, since no penalty is applied for the number of free parameters. To overcome this difficulty, models were ranked using an information criteria approach (Akaike, 1974; Horn, 1987), which has the limitation that the significance level of the ranking is not known. If:

$$\log_e(m_g/m_f) > (k_g - k_f), \quad (2)$$

then model g is ranked above model f, where m_g and m_f are the maximum likelihood estimates for models g and f, and k_g and k_f are the number of free parameters for each scheme.

Tests of whether linear regression slopes were significantly different from zero were made by first obtaining the regression coefficient by fitting with Sigma Plot, and then calculating a t statistic as described by Kleinbaum et al. (1988). Results are expressed as the mean ± SEM.

Estimating the Voltage Sensitivities of the Rate Constants

The voltage sensitivities of the rate constants were estimated using the simplifying assumption of an exponential relationship between the rate constants and membrane potential (Hodgkin and Huxley, 1952; Stevens, 1978; Weiss and Magleby, 1992; Sigworth, 1994):

$$\text{rate}_{ij}(V) = B_{ij} \exp[q_{ij}(V - 30)/k_B T], \quad (3)$$

where $\text{rate}_{ij}(V)$ is the effective rate constant (s^{-1}) for the transition from state i to state j at voltage V (mV), B_{ij} is the value of the base rate constant at +30 mV, q_{ij} is the partial charge (in units of e_O) associated with transition ij, and $k_B T$ is 25.5 mV × units of electronic charge at 23°C. We estimated the value of the base rate at +30 mV to facilitate comparison with rate constants obtained at +30 mV in previous single-channel studies (McManus and Magleby, 1991; Rothberg and Magleby, 1998, 1999).

Since absolute rate theory (Eq. 3) may not necessarily apply to conformational changes in proteins (Eisenberg, 1990; Sigg et al. 1999; Andersen, 1999), the theoretical implications of Eq. 3 should be approached with caution (see Weiss and Magleby, 1992). Nevertheless, such equations can describe the observed experimental observations, and can thus serve as a basis to characterize the voltage-dependent gating of the channel and estimate partial charges associated with various transitions. Alternatively, $q/k_B T$ could be replaced with a constant A, where $1/A$ indicates the voltage sensitivity (see Eq. 6 below), reducing Eq. 3 to an empirical equation that is not dependent on the rate theory assumptions inherent in Eq. 3, except that the dwell times in the various states are exponentially distributed. The final kinetic models would be the same with this substitution, except for the method of expressing the voltage sensitivity of the rate constants.

Estimating Effective Charge Movement q_{eff}

Estimates of lower limits for the effective gating charge q_{eff} were obtained by the limiting slope method (Almers, 1978; Schoppa et al., 1992; Sigworth, 1994; Sigg and Bezanilla, 1997; Horrigan et al., 1999) using log weighting of the open probability, P_o, to emphasize the points at low P_o. This was done by fitting the log of P_o versus voltage with least squares using the Boltzmann equation:

$$P_o = A/\{1 + \exp[-q_{eff}(V - V_{0.5})/(k_B T)]\}, \quad (4)$$

where A is the maximal single-channel open probability, $V_{0.5}$ is the voltage for half-maximal open probability, k_B is the Boltzmann constant, and T is absolute temperature. In cases where a maximal open probability could not be defined due to low levels of activity, this value was fixed to a value of 0.95, which was typical of the maximal P_o for the channel. The limiting slope method of estimating effective gating charge gives the equivalent number of charges for a linear model containing any number of closed states (Almers, 1978). Since the gating of BK channels is inconsistent with linear gating mechanisms (McManus et al., 1985; Rothberg and Magleby, 1998, 1999), estimates of q_{eff} are only effective estimates as related to an assumed linear model.

The effective gating charge q_{eff} is given by Eq. 5:

$$q_{\text{eff}} = ze_o d, \quad (5)$$

where z is the effective valence of the moved charge, e_o is the value of an electronic charge ($e_o = 1.6 \times 10^{-19}$ C), and d is the fractional distance the charge moves in the electric field of the membrane. The voltage sensitivity of the channels, expressed as the change in membrane potential required for an e-fold change in P_o, can be calculated from q_{eff} with:

$$mV/(\text{e-fold change in } P_0) = k_B T/q_{\text{eff}} \quad (6)$$

(Hodgkin and Huxley, 1952). Alternatively, an estimate of q_{eff} for only the effective opening rate or only the effective closing rate, can be determined by rearranging Eq. 6 to solve for q_{eff} from the slope of an exponential fit to the voltage dependence of the mean closed or open times, respectively.

Online Supplemental Material

Fig. S1 presents single-channel currents simulated over a range of Ca^{2+}_i and voltage using Scheme II. The noise and filtering used in the simulation was equivalent to that in the experimental current records to allow direct comparison to the experimental records in Fig. 1. The simulated single-channel current records in Fig. S1 were essentially indistinguishable from the experimental current records in Fig. 1, except for stochastic variation and a slightly more stable baseline in the simulated data. Thus, comparison of simulated to experimental data shows that Scheme II predicted the characteristic features of the single-channel current records over wide ranges of voltage (−80 to +70 mV) and Ca^{2+}_i (~0 to 1,024 μM). Fig. S1 is available online at http://www.jgp.org/cgi/content/full/116/1/75/DC1

RESULTS

Currents through a single large-conductance Ca^{2+}-activated K^+ channel at two different Ca^{2+}_i, each at three different voltages ranging from +30 to +50 mV, are shown in Fig. 1 A. These traces illustrate the activation of the channel by both Ca^{2+}_i and depolarization. The activating effect of Ca^{2+}_i at three different voltages can be seen by comparing each trace on the left with the corresponding trace on the right at higher Ca^{2+}_i. At +30 mV, increasing Ca^{2+}_i from 5.5 to 12.3 μM increased P_o 8.3-fold, from 0.024 to 0.20. Similarly, the activating effect of voltage can be seen by comparing the top traces with the traces below. For example, at 5.5 μM Ca^{2+}_i, changing the voltage from +30 to +50 mV increased P_o 9.2-fold, from 0.024 to 0.22.

Voltage also modulated BK channels at the extremes of very high and very low Ca^{2+}_i. Fig. 1 C shows that depolarizing from −80 to −50 mV in very high (1,024 mM) Ca^{2+}_i increased P_o 8.5-fold, from 0.026 to 0.22. Fig. 1, B and D, presents examples of data recorded at very low Ca^{2+}_i, of 0.0003 (C) and 0.03 μM (D). Such low Ca^{2+}_is are effectively equivalent to ~0 Ca^{2+}_i (Meera et al., 1996; Cui et al., 1997; Nimigean and Magleby, 2000), and within the limits of stochastic variation, channel activity in 0.0003 and 0.03 μM Ca^{2+}_i appeared similar. Fig. 1 B presents selected channel openings with 0.0003 μM Ca^{2+}_i on a time base to allow direct comparison to the currents in A and C. Fig. 1 D presents currents recorded with 0.03 μM Ca^{2+}_i on a very slow time base to show the low frequency of channel opening at very low Ca^{2+}_i. The insets on a much faster time base show that openings can still occur in bursts at very low Ca^{2+}_i. In spite of the low activity, increasing the voltage from +30 to +70 mV increased P_o an average of ~25-fold in the overall records from which the examples shown in Fig. 1, B and D, were taken.

Voltage Dependence of BK Channel Activation

Insight into the voltage dependence of channel opening can be obtained from fitting the steady state P_o vs. voltage relation with a Boltzmann distribution (Hodgkin and Huxley, 1952). We used log-weighting to obtain the best Boltzmann fit of the data obtained at low P_o to estimate q_{eff} from the limiting slope (Almers, 1978), where q_{eff} is the effective charge movement associated with activation. Because of the complex gating mechanism of BK channels, with two or more separate transition pathways connecting multiple open and closed states (McManus and Magleby, 1991; Rothberg and Magleby, 1998, 1999), it might be expected that limiting slope measurements would give an underestimation of the actual charge movement involved in the full activation of the channels (Horrigan et al., 1999). Nevertheless, estimates of the limiting slope can give a measure of effective charge movement and can be used to examine the effects of Ca^{2+}_i on the voltage dependence of the gating. (For further discussions of the limiting slope method and its limitations, see Almers, 1978; Schoppa et al., 1992; Sigworth 1994; Sigg and Bezanilla, 1997.)

Examples of data used to estimate limiting slope are shown in Fig. 2, A and B, which plots on linear and logarithmic coordinates steady state P_o vs. voltage for single-channel data recorded from five different single-channel patches at each of four different Ca^{2+}_i. Boltzmann fits to the data (Eq. 4) are plotted as thick continuous lines. Increasing Ca^{2+}_i shifts the P_o–V relation leftward on the voltage axis (Barrett et al., 1982; Latorre et al., 1982; Cox et al., 1997).

The limiting slopes are more clearly seen in Fig. 2 B, where the logarithmic coordinates emphasize the data obtained at low P_o. Changing Ca^{2+}_i ~30,000-fold had little apparent effect on the limiting slope over the examined range of P_os. Fig. 2 C plots 17 estimates of q_{eff} against Ca^{2+}_i for data from five different single BK channels and also from two patches containing four BK channels each. The mean estimate of q_{eff} was 2.3 ± 0.6 e_o (thick line), giving an e-fold increase in P_o per 11.1 mV depolarization. There was little effect of Ca^{2+}_i on q_{eff}, as the slope of a linear regression line (−0.025 e_0/10-fold increase in Ca^{2+}_i, not shown) was not significantly different from zero ($P > 0.45$), and the correlation coefficient ($r^2 = 0.006$) was negligible. These results suggest that changes in Ca^{2+}_i have little effect on the effective gating charge, as measured in these experiments. This mean

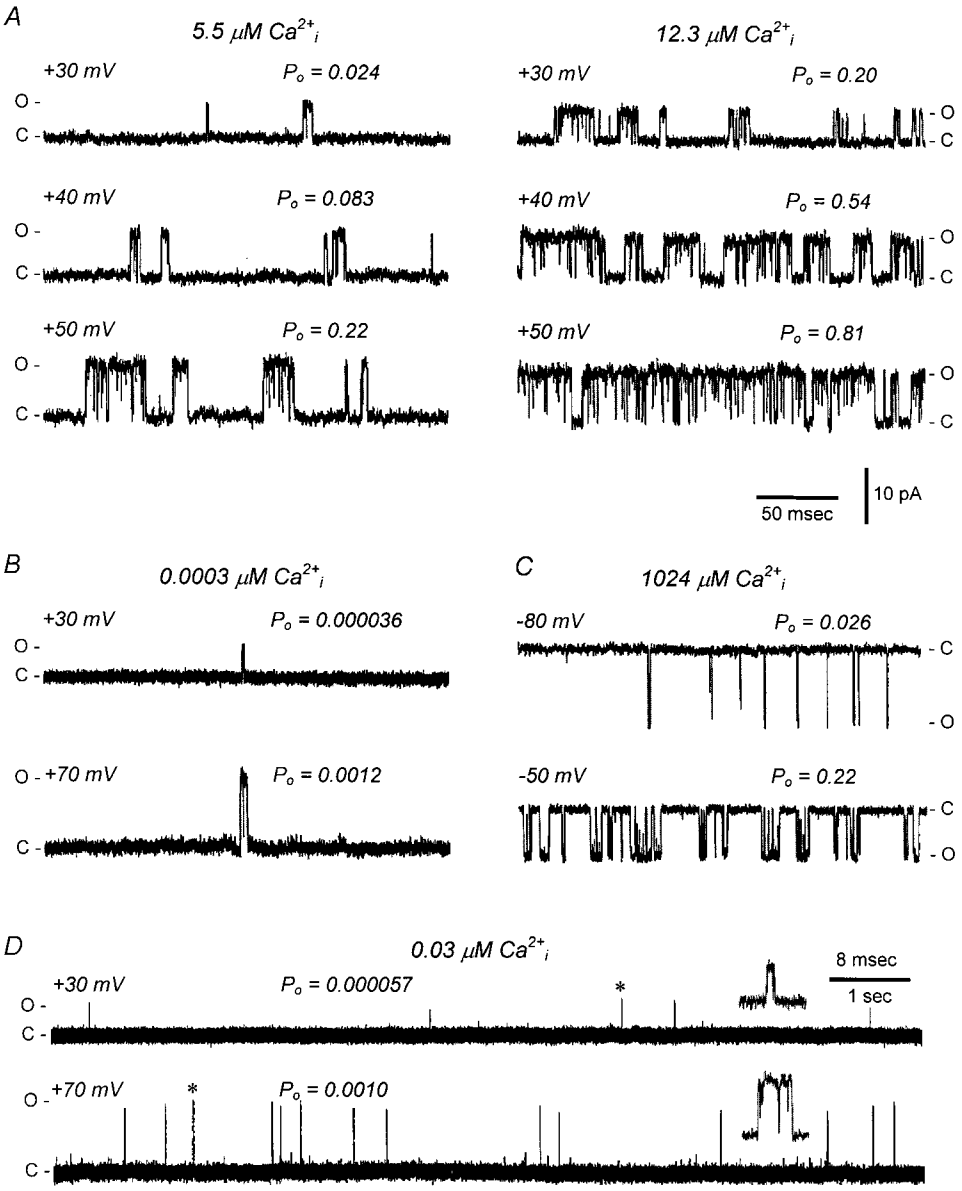

Figure 1. Single-channel currents recorded over a range of Ca^{2+}_i and voltage show that BK channels are activated by both depolarization and Ca^{2+}_i. The open (O) and closed (C) current levels are indicated, where upward current steps indicate channel opening at positive potentials and downward current steps indicate channel opening at negative potentials. (A) Activation by Ca^{2+}_i and voltage in the intermediate range of Ca^{2+}_i. Depolarization increases P_o (compare the traces at +30 mV with the traces at +40 and +50 mV), and increased Ca^{2+}_i increases P_o (compare traces at 5.5 μM with traces obtained at the same voltages at 12.3 μM Ca^{2+}_i). Channel B13. (B) Depolarization increases P_o at very low (essentially zero) Ca^{2+}_i. Representative openings are shown as the closed intervals were typically 1–2 s in duration. Channel B14. (C) Depolarization from −80 to −50 mV activates BK channels at high (saturating) Ca^{2+}_i. Channel B16. (D) Longer current traces (10 s) are displayed at a slower time base to illustrate that depolarization increases the frequency of opening at very low Ca^{2+}_i. *Bursts of openings are shown at a fast time base above each trace at the right. Channel B14.

estimate of q_{eff} of 2.3 e_O obtained from limiting slope measurements of single-channel data can be compared with the estimates for h*Slo* of 1.6 e_O (Diaz et al., 1998) and for *mSlo* of ~2 e_O (Horrigan et al., 1999) obtained over a similar range of P_o. For levels of $P_o < \sim 10^{-4}$, the limiting slope becomes more shallow (Horrigan et al., 1999), suggesting less charge movement for activation at hyperpolarized voltages in ~0 Ca^{2+}_i.

The effect of Ca^{2+}_i on $V_{1/2}$ values (the voltage for half-maximal activation) estimated from the same data used for Fig. 2 C is shown in Fig. 2 D. In the range of 4–1,000 μM, increasing Ca^{2+}_i shifted $V_{1/2}$ towards more hyperpolarized voltages with a slope of −50 mV per 10-fold increase in Ca^{2+}_i (thick line). In contrast, $V_{1/2}$ was independent of Ca^{2+}_i at very low Ca^{2+}_i, where a 100-fold increase in Ca^{2+}_i from 0.3 to 30 nM had little effect on the $V_{1/2}$ of 150 mV (horizontal thick line). This apparent lack of effect of Ca^{2+}_i on $V_{1/2}$ at very low Ca^{2+}_i is consistent with observations in previous studies using macroscopic currents recorded from h*Slo* (Meera et al., 1996), and suggests that BK channels contain an intrinsic voltage sensor that does not require Ca^{2+}_i to couple voltage to channel opening (Meera et al., 1996; Cox et al., 1997; Stefani et al., 1997; Horrigan et al., 1999; Horrigan and Aldrich, 1999).

Wei et al. (1994) and Cui et al. (1997) have observed that the $V_{1/2}$ vs. log Ca^{2+}_i relationship becomes less steep for $Ca^{2+}_i > \sim 100$ μM. Our observations in Fig. 2 D are not sufficient to confirm this decrease in slope because of the scatter in the data. Cui et al. (1997) have argued that this decreased slope at higher Ca^{2+}_i can be taken as evidence against a model considered by Moczydlowski and Latorre (1983) in which the voltage dependence of the channel

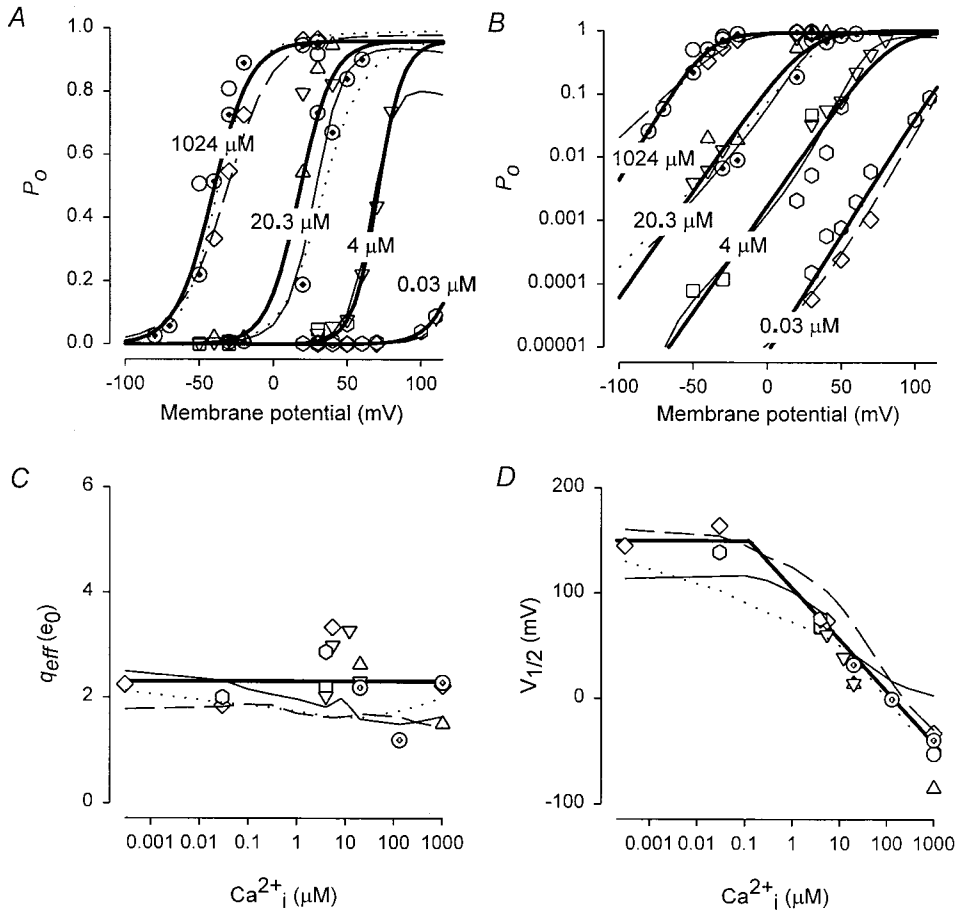

Figure 2. Increasing Ca^{2+}_i shifts voltage-activation curves to more hyperpolarized potentials, while having little effect on the apparent limiting slope. (A) P_O vs. voltage is plotted on a linear scale for data obtained from two to three different single-channel patches at each Ca^{2+}_i. The continuous thick lines are fits with the Boltzmann equation: $P_o = A/\{1 + \exp[q_{eff}(V - V_{1/2})/k_BT]\}$, where A was usually fixed at 0.95 (the maximum P_o typically observed for these channels). The thin continuous, dashed, and dotted lines represent curves predicted by Q-matrix calculations using Scheme II for channels B13, B14, and B16, respectively. (B) Data from A replotted on semilogarithmic coordinates, to emphasize data at very low P_o used in limiting slope estimates. The Boltzmann fits are different from those in A due to the log-weighting used to emphasize the data at low open probability to estimate the limiting slope. (C) Effective gating charge per channel (q_{eff}) vs. Ca^{2+}_i. q_{eff} was estimated from individual Boltzmann fits obtained from 16 different P_o vs. voltage curves. The thick solid line represents the mean q_{eff}. (D) Plot of the voltage for half-maximal P_o ($V_{1/2}$) vs. Ca^{2+}_i, estimated from the same Boltzmann fits used for C. $V_{1/2}$ was insensitive to Ca^{2+}_i for $Ca^{2+}_i \leq 0.03$ μM, but decreased steeply with Ca^{2+}_i from 4 to 1,000 μM. Symbols in A–D represent channels B07 (○), B10 (□), B11 (△), B13 (▽), B14 (◇), B15 (hexagons), and B16 (⊙). The thin lines in C and D represent predictions using Scheme II for channels B13 (continuous line), B14 (dashed line), and B16 (dotted line).

arises from voltage altering the concentration of Ca^{2+}_i at binding sites located within the electric field of the membrane. An additional compelling argument against such a model is the observation in Fig. 2 D and in previous experiments (Meera et al., 1996; Rothberg and Magleby, 1996; Cui et al., 1997; Nimigean and Magleby, 2000) that the gating becomes insensitive to Ca^{2+}_i at low Ca^{2+}_i. If voltage acted through altering the concentration of Ca^{2+} at binding sites within the electric field, then estimates of $V_{1/2}$ should not become independent of Ca^{2+}_i at low Ca^{2+}_i.

Voltage-dependence of Mean Open and Closed Intervals

To gain further insight into the voltage dependence of the gating transitions, the mean durations of open and closed intervals were measured over a range of voltages and Ca^{2+}_i. Fig. 3, A and B, presents such data at three different Ca^{2+}_i from three representative channels. Both depolarization and Ca^{2+}_i increased mean open times and decreased mean closed times. The voltage dependence of mean open times could be approximated by single exponentials over the examined range of Ca^{2+}_i and voltage (thick lines). In contrast, the mean closed times were first approximated by a single exponential, and then approached a minimum of ~180 μs under conditions of voltage and Ca^{2+}_i when $P_o > 0.95$ (thick lines). As will be shown in a later section, a minimum mean closed time is reached because the dominant closed intervals at high P_o are the flickers (brief closings within bursts), which have observed mean lifetimes that are little affected by voltage.

The slopes of the exponential part of the thick lines in Fig. 3, A and B, give a measure of the voltage dependence of the apparent mean closing and opening rates, respectively (see methods). Estimates of the effective charge movement q_{eff} determined from plots of this type are presented in Fig. 3 C. The mean q_{eff} associated with channel closing, as determined from the open durations, was -0.5 e_O, giving an e-fold decrease in closing rate per 50-mV depolarization (dashed line through open symbols in Fig. 3 C), and the mean q_{eff} associated with channel opening, as determined from the

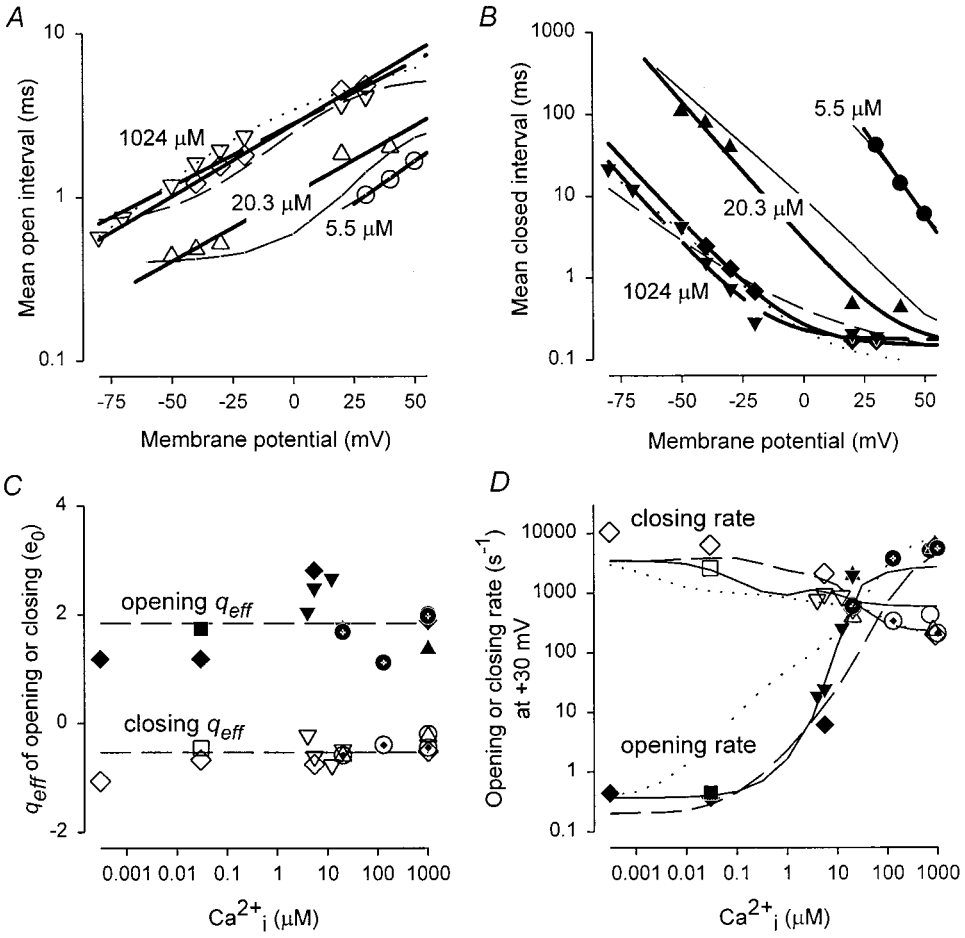

Figure 3. Effects of voltage and Ca^{2+}_i on mean open- and closed-interval durations. (A) Semilogarithmic plots of mean open-interval duration vs. voltage at 5.5, 12.3, and 1,024 μM Ca^{2+}_i for channels B13 (○ and △), B14 (◇) and B16 (▽). The thick lines at each Ca^{2+}_i are fits with single exponentials, and the thin continuous, dashed, and dotted lines represent predicted mean open interval vs. voltage obtained by simulation of Scheme II (with filtering and noise; see methods) for channels B13, B14, and B16, respectively. (B) Semilogarithmic plots of mean closed-interval durations vs. voltage at 5.5, 12.3, and 1,024 μM Ca^{2+}_i for the same three channels in A. Lines through each set of points indicate fits with a single exponential, plus a baseline term to account for the minimum mean closed-interval observed at higher Ca^{2+}_i. The thin continuous, dashed, and dotted lines represent predicted mean closed interval vs. voltage obtained by simulation of Scheme II for channels B13, B14, and B16, respectively. (C) Effective gating charge (q_{eff}) estimated from 16 individual exponential fits of mean open and closed intervals vs. voltage, plotted as a function of Ca^{2+}_i. The dashed lines at −0.5 and +1.8 indicate the mean q_{eff} for channel closing (determined from the voltage dependence of the mean open intervals) and channel opening (determined from the voltage dependence of the mean closed intervals), respectively. (D) Semilogarithmic plot of the mean opening and closing rates (1/mean closed or open intervals) at +30 mV plotted as a function of Ca^{2+}_i. Thin lines represent predicted values obtained from Q-matrix calculations using Scheme II (with correction for missed events) for channels B13, B14, and B16.

closed durations, was 1.8 e_O, giving an e-fold increase in opening rate per 14-mV depolarization (dashed line through filled symbols). The plots in Fig. 3, A–C, show that the effective charge movement associated with opening and closing is relatively independent of voltage or Ca^{2+}_i over the examined range of conditions.

Fig. 3 D plots the apparent mean closing and opening rates at +30 mV as a function of Ca^{2+}_i. The apparent mean opening rate (determined from the inverse of the closed-interval durations) was steeply Ca^{2+} dependent over the examined range of ~1–50 μM Ca^{2+}_i. Outside of this range, the apparent mean opening rate was little affected by Ca^{2+}_i, reaching an observed minimum of ~0.5/s at very low Ca^{2+}_i and an observed maximum of ~5,500/s at high Ca^{2+}_i. The maximum Ca^{2+} dependence of the apparent mean closing rate (determined from the inverse of the open interval durations) was considerably less than for the apparent mean opening rate, as indicated by the open symbols in Fig. 3 D. The results in Fig. 3 D are consistent with previous observations (Rothberg and Magleby, 1999) showing that the single-channel kinetics become relatively Ca^{2+} insensitive at high Ca^{2+}_i (100–1,024 μM), and more extensive observations than presented here (Nimigean and Magleby, 2000; observations on *mSlo*) also indicate that the single-channel gating kinetics are relatively independent of Ca^{2+} at very low Ca^{2+}_i (<0.1 μM).

Voltage Shifts the Open and Closed Dwell-time Distributions

To obtain further insight into the effects of voltage on the transitions among states, the open and closed intervals were binned into dwell-time distributions and fitted with sums (mixtures) of exponential components. The numbers of significant exponential components give an estimate of the minimal number of states entered during gating (Colquhoun and Hawkes, 1995a). Open dwell-time distributions obtained at +30 and +50 mV at two different Ca^{2+}_i of 5.5 and 12.3 μM are shown Fig. 4, A–D. Over the 34-fold range in P_o in these experiments (from 0.024 to 0.81), each of the open distributions was

best fit with the sum of three exponential components (thin continuous lines), suggesting that neither voltage nor Ca^{2+}_i changed the minimal numbers of detected open states entered over these experimental conditions.

The fits to the open distributions obtained at +30 mV in Fig. 4, A and B, are plotted as dashed lines on the open distributions obtained at +50 mV in Fig. 4, C and D, at the same Ca^{2+}_i. It can be seen that the major effects of the additional depolarization were to increase the number and duration of the longer openings while decreasing the number of the briefer open intervals.

Closed dwell-time distributions from the same experiment are shown in Fig. 4, E–H. The closed distributions at the lower P_os of 0.024, 0.20, and 0.22 (E–G) were best fit by the sums of five exponential components, and the distribution at the higher P_o of 0.81 (H) was best fit with the sum of four exponential components (thin continuous lines), suggesting that a minimum of four to five closed states are entered during gating over the wide examined range of P_o.

The fits to the closed distributions obtained at +30 mV (Fig. 4, E and F) are plotted as dashed lines on the closed distributions obtained at +50 mV (G and H) at the same Ca^{2+}_i. The major effects of further depolarization were to greatly decrease the durations and frequency of the longer closed intervals, shifting the area to the briefer closed intervals. The shifts in the closed distributions with depolarization were more pronounced than for the open distributions, consistent with the greater voltage dependence of the mean closed-interval duration when compared with the mean open-interval duration (Fig. 3).

For data obtained from six additional channels with one to four different Ca^{2+}_i for each channel, at least three to four open and four to six closed states were typically entered during gating over the examined ranges of P_o. In these additional experiments, as was the case for Fig. 4, there was no obvious effect of voltage on estimates of the numbers of states.

Fig. 5 plots representative examples of the effect of voltage on the time constants and areas of the longest and briefest duration exponential components (filled and open symbols, respectively) for both the open and closed dwell-time distributions for data obtained at 4.0, 20.3, and 1,024 μM Ca^{2+}_i. The time constant of the longest open component increased with depolarization (Fig. 5 A), while the time constant of the longest closed component decreased with depolarization (B), and this was the case over the range of examined Ca^{2+}_i. In contrast, the time constants of the briefest open and closed components were little affected by depolarization for any given channel. For the low and intermediate levels of Ca^{2+}_i, depolarization shifted area from the briefest open intervals towards the longest open intervals and from the longest closed intervals towards the briefest closed intervals (Figs. 5, C and D).

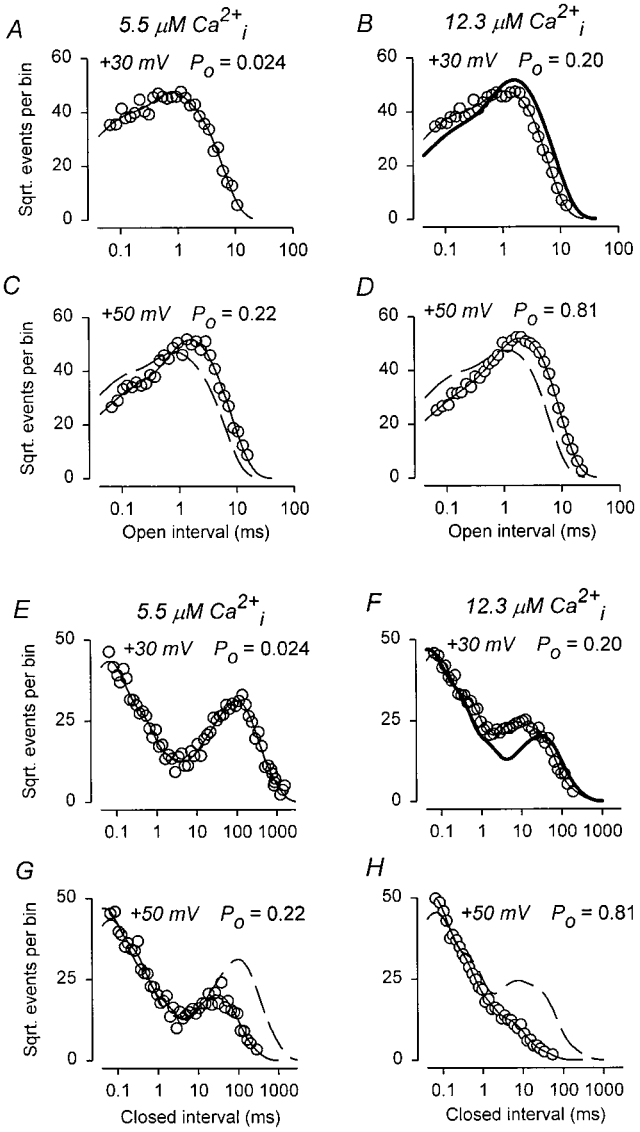

Figure 4. Voltage- and Ca^{2+}-induced shifts in the open and closed dwell-time distributions. (A–D) Open dwell-time distributions at +30 and +50 mV for 5.5 and 12.3 μM Ca^{2+}_i. The thin continuous lines are fits to the distributions with the sums of three exponential components. The dashed lines in C and D plot the fits to the distributions obtained at +30 mV on the data obtained at +50 mV at the same Ca^{2+}_i. The thick line in B plots the fit to the distribution in C on the distribution in B. Open distributions obtained at similar P_os, but with different Ca^{2+}_i and voltage, are different. (E–H) Open dwell-time distributions at +30 and +50 mV for 5.5 and 12.3 μM Ca^{2+}_i. The thin continuous lines are fits to the distributions with the sums of five exponential components. The dashed lines in G and H plot the fits to the distributions obtained at +30 mV on the data obtained at +50 mV at the same Ca^{2+}_i. The thick line in F plots the fit to the distribution in G on the distribution in F. Closed distributions obtained at similar P_os but different Ca^{2+}_i and voltage are different. The numbers of fitted intervals in the distributions were: A, 3,061; B, 5,098; C, 2,384; D, 13,570; E, 2,617; F, 4,248; G, 1,838, and H, 9,728. To facilitate comparison between the dwell-time distributions in this and the following figures, the numbers of intervals in each distribution have been normalized to 100,000 for time ranging from 0 to infinity. Channel B13.

(The effects of voltage on the intermediate components was more variable and will not be considered here.)

Voltage and Ca^{2+}_i Have Differential Effects on the Gating Kinetics

Data were presented in a previous section suggesting that the voltage dependence of the channel does not arise through voltage-induced alterations in the concentration of Ca^{2+}_i at binding sites located within the electric field of the membrane, consistent with previous studies (Wu et al., 1995; Meera et al., 1996; Rothberg and Magleby, 1996; Cox et al., 1997; Cui et al. 1997; Diaz et al., 1998; Horrigan et al., 1999; Horrigan and Aldrich, 1999). The arguments were based on data obtained at very low and very high Ca^{2+}_i. This section further tests this hypothesis under conditions of intermediate levels of Ca^{2+}_i. If voltage acts only through changing Ca^{2+}_i at the Ca^{2+}-binding sites, then activating the channel by depolarization would change only the rate (but not the second-order rate constant) of Ca^{2+} binding. In this case, depolarization should have the same effects on the gating kinetics as an increase in Ca^{2+}_i, as both methods would increase the rate of Ca^{2+} binding while having no effect on any rate constants. To test whether the gating kinetics are the same for activation by either voltage or Ca^{2+}_i, we compared open and closed dwell-time distributions for data with the same P_o, but with different levels of Ca^{2+}_i and voltage. Representative results are shown in Fig. 4, B and F.

The thick line in Fig. 4 B plots the open dwell-time distribution obtained at +50 mV with 5.5 μM Ca^{2+}_i on the open distribution obtained at +30 mV with 12.3 μM Ca^{2+}_i. The P_os under these two sets of conditions were similar (0.22 vs. 0.20). Increasing Ca^{2+}_i and then decreasing depolarization to obtain the same P_o shifted the open distribution to the left, with a decreased frequency of the longer open intervals and an increased frequency of the briefer open intervals. The thick line in Fig. 4 F plots the closed dwell-time distribution obtained at +50 mV with 5.5 μM Ca^{2+}_i on the closed distribution obtained at +30 mV with 12.3 μM Ca^{2+}_i. For the closed distribution, increasing Ca^{2+}_i and then decreasing the depolarization to obtain the same P_o greatly increased the frequency of the closed intervals with durations from 1 to 20 ms and slightly decreased the durations of the longer closed intervals. The differences in the open and closed distributions were not due to the small difference in P_o, as shifting either voltage or Ca^{2+}_i sufficiently to change the P_o ~10% of its internal value had little effect on the distributions.

The marked changes in the dwell-time distributions in Fig. 4 when changing voltage and Ca^{2+}_i to maintain the same P_o indicates that depolarization does not have the same effects on single-channel kinetics as increasing

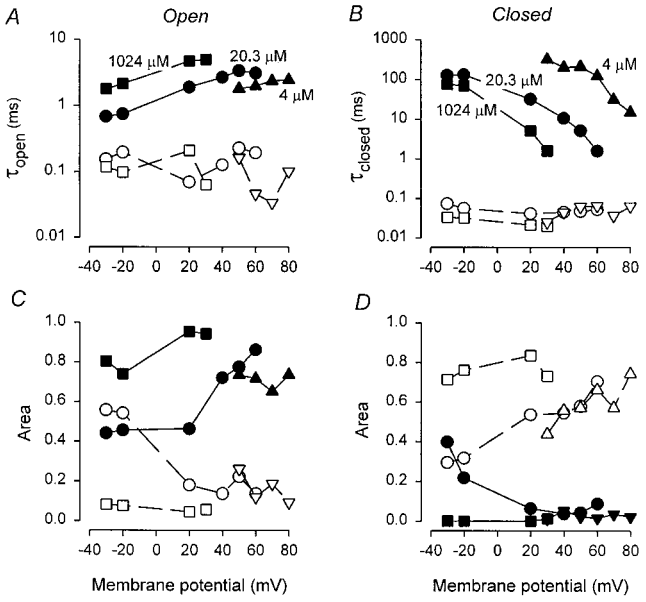

Figure 5. Effects of Ca^{2+}_i and voltage on the time constants and areas of the longest and briefest exponential components describing the open and closed dwell-time distributions. (A) Time constants of the longest (solid symbols) and briefest (open symbols) components of open dwell-time distributions at 4 (up triangles, B13), 20.3 (circles, B16) and 1,024 (squares, B14) μM Ca^{2+}_i. (C) Areas of corresponding components in A. Depolarization generally increased the durations and areas of longest open component. (B and D) Time constants and areas of the longest and briefest components of closed dwell-time distributions. Depolarization generally decreased the durations and areas of the longest closed component.

Ca^{2+}_i. Similar shifts in the shapes of the distributions obtained at the same P_o, but with different Ca^{2+}_i and voltage, were found in four additional comparisons from three additional channels for P_os ranging from 0.18 to 0.89, Ca^{2+}_i ranging from 5.5 to 1,024 μM, and voltage ranging from −20 to +50 mV. In all comparisons, increasing Ca^{2+}_i and decreasing depolarization to obtain the same P_o decreased the observed mean durations of both the open and closed intervals. For example, in Fig. 4, B and F, increasing Ca^{2+}_i from 5.5 to 12.3 μM and changing the voltage from +50 to +30 mV decreased the observed mean durations of both the open and closed interval durations ~30%. As another example, in an experiment on a different patch, increasing Ca^{2+}_i from 20.3 to 132 μM and changing the voltage from +20 to −30 mV to maintain the P_o at ~0.19 decreased the observed mean open and closed interval durations ~17%. The differential effects of voltage and Ca^{2+}_i on the single-channel kinetics at intermediate levels of Ca^{2+}_i shown in this section provides further evidence that voltage does not activate the channel solely through changes in the effective Ca^{2+}_i at the Ca^{2+}-binding sites. Note that this conclusion applies to the limited case where voltage acts only by changing Ca^{2+}_i at its binding

sites without changing any of the rate constants. Consequently, it does not exclude more complicated mechanisms in which voltage acts through both changes in $Ca^{2+}{}_i$ at the binding sites and changes in rate constants.

Working Hypothesis for Voltage Dependent Gating

Any viable model for the gating of BK channels must account for the properties of the voltage dependence described above and also the properties of the $Ca^{2+}{}_i$ dependence. We have recently suggested that the Ca^{2+} dependence of the gating is consistent with the 50-state model shown in Scheme I, in which the top tier of states are closed and the bottom tier of states are open (Rothberg and Magleby, 1999). The tetrameric structure of the channel (Shen et al., 1994) is reflected in the four subunits comprising each state of the channel, with each subunit capable of binding at least one Ca^{2+} (Wei et al., 1994; Schreiber and Salkoff, 1997; Schreiber et al., 1999). Subunits with a bound $Ca^{2+}{}_i$ are indicated by shading. $Ca^{2+}{}_i$ binding shifts the gating towards the right hand side of the scheme, as indicated. Each subunit can undergo a conformational change (indicated by the transitions between the squares and circles) with or without bound $Ca^{2+}{}_i$. In terms of this model, it is the conformational changes of the various subunits together with the opening and closing conformational changes that generate the multiple open and closed states that the channel can enter at nominally zero $Ca^{2+}{}_i$ (Horrigan et al., 1999; Horrigan and Aldrich, 1999; Nimigean and Magleby, 2000; Talukder and Aldrich, 2000) and also very high $Ca^{2+}{}_i$ (Rothberg and Magleby, 1999). The large numbers of states on each tier arise from the various combinations of subunit conformations and different numbers of bound $Ca^{2+}{}_i$.

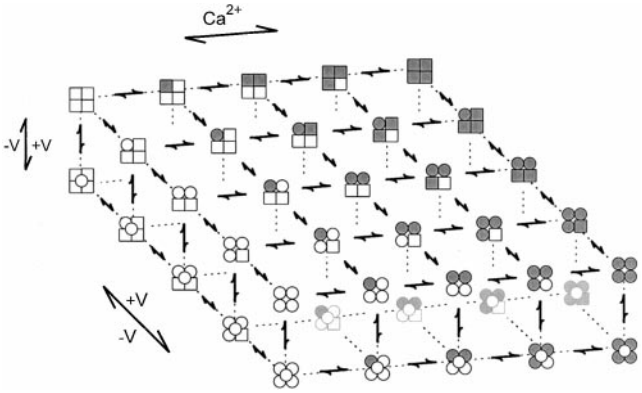

(SCHEME I)

In the context of Scheme I, the voltage dependence of activation could arise through voltage-dependent Ca^{2+}-binding steps or voltage-dependent conformational changes not related to Ca^{2+} binding. The results in this (Figs. 2–4) and previous (Meera et al., 1996; Rothberg and Magleby, 1996; Cox et al., 1997; Cui et al. 1997; Diaz et al., 1998; Horrigan et al., 1999; Horrigan and Aldrich, 1999) studies have shown that the voltage activation of BK channels is an intrinsic property of the channel and does not arise through voltage-dependent increases in Ca^{2+} binding. Consistent with this conclusion, BK channels show homology to the superfamily of voltage-gated K^+ channels, including an S4 voltage sensor (Atkinson et al., 1991; Adelman et al., 1992; Butler et al., 1993; Pallanck and Ganetzky, 1994; Diaz et al., 1998), and also display gating currents in the absence of $Ca^{2+}{}_i$ (Stefani et al., 1997; Horrigan and Aldrich, 1999).

For separate voltage- and Ca^{2+}-dependent steps, the voltage activation would arise through one or more voltage-dependent conformational changes separate from the Ca^{2+}-dependent transitions in Scheme I. Thus, depolarization could activate the channel by driving the conformational change from the closed states on the upper tier to the open states on the lower tier (as indicated by the vertical arrow in Scheme I), by driving the conformational changes of the individual subunits for transitions among states within each tier (as indicated by the oblique voltage arrow in Scheme I), or by driving both of these types of conformational changes. To distinguish among these possibilities, the complex Scheme I was simplified by reducing the numbers of states to decrease the numbers of free parameters. If the simpler scheme could account for the single-channel data, then the more complex Scheme I should also be able to account for the data.

Based on our previous study of the Ca^{2+}-dependent gating (Rothberg and Magleby, 1999), Scheme I was reduced to Scheme II by condensing three rows of intermediate open states in Scheme I into one row of intermediate open states and by condensing three rows of intermediate closed states into one row of intermediate closed states. An additional row of open states has also been excluded by assuming that they are entered infrequently under the conditions of the present studies. However, occasional entry into these states may be expected at hyperpolarized voltages (Horrigan et al., 1999). With these simplifying assumptions, Scheme II can serve as a starting point to examine possible mechanisms for the voltage dependence of the single-channel gating.

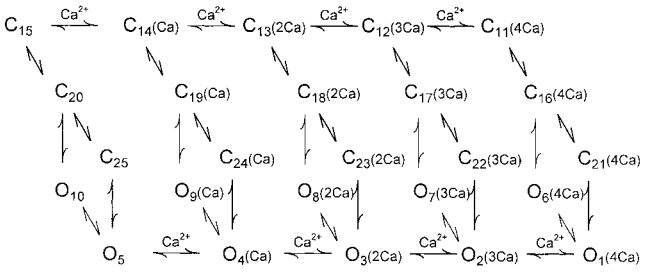

(SCHEME II)

Note that Schemes I and II each consist of five parallel subschemes, with either 0, 1, 2, 3, or 4 Ca^{2+} bound to each state. For Scheme I, each subscheme is comprised of five closed and five open states, and, for Scheme II, each subscheme is comprised of three closed and two open states, as shown by Scheme III.

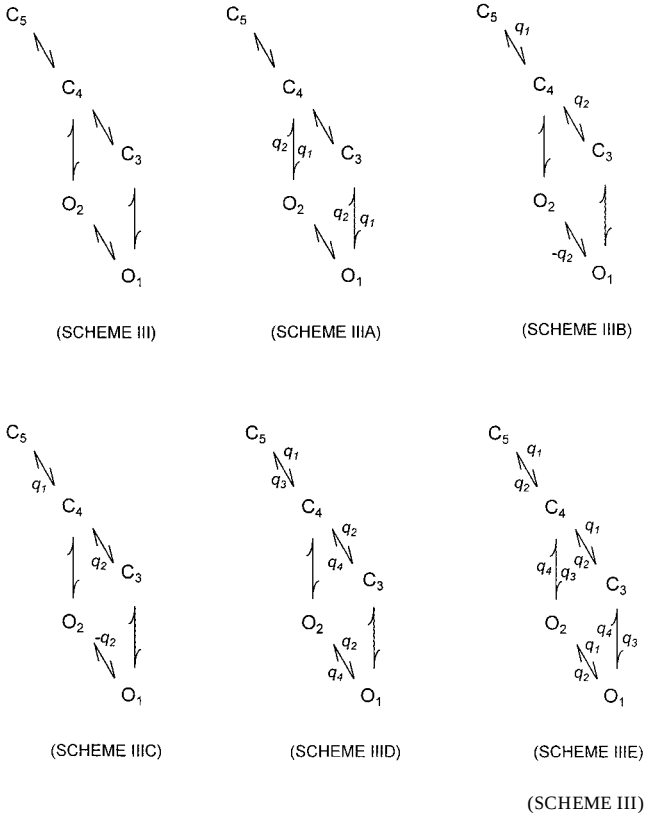

Our general approach to testing Scheme II quantitatively was to estimate the most likely rate constants for this scheme, including their Ca^{2+}_i and voltage dependence, and then to determine whether Scheme II, with the most likely rate constants, could account for the Ca^{2+}_i and voltage dependence of the single-channel data. To do this, we first examined which of the transitions in Scheme II were voltage dependent. This was done by examining the voltage dependence of the gating in the limiting cases of $\sim$0 Ca^{2+}_i and saturating Ca^{2+}_i, to confine the gating to subsets of states within Scheme II with either zero or four bound Ca^{2+}, respectively.

Identifying the Voltage-dependent Transitions within the Subscheme of Unliganded States

The observation that $V_{1/2}$ at very low Ca^{2+}_i ($\leq$0.03 μM) is essentially independent of Ca^{2+} (Fig. 2 D; Meera et al., 1996) suggests that Ca^{2+} binding is infrequent under such low Ca^{2+} conditions. On this basis, channel activity for $Ca^{2+}_i \leq 0.03$ μM would reflect mainly the gating among the unliganded states, given by the left-most subscheme in Scheme II. Since Scheme III is identical to the left-most subscheme in Scheme II, identifying the voltage-dependent transitions for Scheme III under conditions where $Ca^{2+}_i \leq 0.03$ μM should then identify the voltage-dependent transitions for the unliganded states in Scheme II.

Five different forms of Scheme III were examined in which the voltage dependence of the various rate constants, indicated by q_1–q_4, was constrained in different ways, as shown in Scheme III (A–E). Rate constants without an associated q have no voltage dependence. Three estimates of the most likely rate constants and their voltage dependence were obtained for the unliganded channel for each form of Scheme III. Each estimate was obtained by simultaneously fitting 2-D dwell-time distributions obtained at three different voltages (+30, +50, and +70 mV). One of the estimates was obtained from channel B15 for Ca^{2+}_i of 0.03 μM, and the other two were obtained from channel B14 for Ca^{2+}_i of 0.03 and 0.0003 μM. (The number of interval pairs fitted in each 2-D dwell-time distribution in these experiments ranged from 65 to 793.)

Fitting sums of exponential components to the dwell-time distributions in these experiments indicated typically two significant open components and two to three significant closed components for unliganded gating. Similar experiments on *mSlo* analyzing greater numbers of intervals detected two to three open and three to five closed components in $\sim$0 Ca^{2+}_i (Nimigean and Magleby, 2000; Talukder and Aldrich, 2000). Taken together, these findings suggest gating among a minimum of two to three open and three to five closed states at $\sim$0 Ca^{2+}_i.

Table I presents the normalized likelihood ratios for one interval pair, NLR_1, to give a measure of how well the various models described the data. The NLR_1 gives the ratio of the likelihood for fitting with the model to the likelihood for the theoretical best description of the data, normalized to one open–closed interval pair. [See methods and Rothberg and Magleby (1998, 1999) for detailed discussions of the NLR and how the theoretical best description can be obtained.] A NLR_1 of 1.0 would indicate that the model describes the data as well as the theoretical best description of the data, and a NLR_1 of 0.95 would indicate that there is an average difference in likelihood of 5% per interval pair between the predicted distributions and the theoretical best description. Since the NLR gives an average for interval pairs, the likelihood difference could be greater than this for some areas of the distribution and less for others.

The rankings of the schemes based on the Akaike criteria, which applies a penalty for additional free parameters (Eq. 2), are also listed in Table I. Scheme III A, with only the open–closed transitions being voltage de-

TABLE I

NLR_1 and Rankings (R) of Scheme III, A–E

	Unliganded states						Fully liganded states					
	Channel B15		Channel B14		Channel B14		Channel B16		Channel B07		Channel B14	
Scheme III	0.03 μM Ca^{2+}_i		0.03 μM Ca^{2+}_i		0.0003 μM Ca^{2+}_i		1024 μM Ca^{2+}_i		1024 μM Ca^{2+}_i		1024 μM Ca^{2+}_i	
	NLR_1	R	NLR_1	R	NLR_1	R	NLR_1	R	NLR_1	R	NLR_1	R
A	0.963	5	0.955	5	0.967	4	0.846	5	0.952	5	0.938	5
B	0.990	3	0.958	3	0.976	1	0.925	4	0.964	4	0.940	4
C	0.966	4	0.955	4	0.945	5	0.942	3	0.968	3	0.942	3
D	0.992	2	0.961	2	0.976	3	0.944	2	0.969	2	0.947	2
E	0.992	1	0.963	1	0.978	2	0.965	1	0.975	1	0.970	1

pendent, gave the worst or next to worst descriptions of the data (lowest values for the log likelihood and NLR_1) and also ranked the lowest (5th) or next to lowest (4th). Scheme III E, with voltage dependence in each rate constant, gave the best description of the data in each case (highest values for the NLR_1) and ranked highest for two estimates and second highest for one estimate. Since all of the schemes are nested, the likelihood ratio test can be used to determine which of the rankings are significant (Horn, 1987) for the unliganded gating. Scheme III E ranked significantly ($P < 0.05$) above A–C, except for B for channel B14 at 0.0003 μM Ca^{2+}_i. The rankings of Scheme III E over D were not significant. The ranking of B over E for channel B14 at 0.0003 μM Ca^{2+}_i was not significant.

The mean ± SEM of the estimated rate constants and their voltage dependence for Scheme III E are shown in Table II. Although estimates of some of the rate constants were consistent among the three sets of data, others showed large variability from being poorly defined, due in part to the very limited amount of data that was obtained at the low P_os associated with the very low Ca^{2+}_i. For the well-defined rate constants, the transition from C5 to C4 was consistently slow at ~2/s, generating the long closed intervals, and transitions such as O1–C3–O1 generated most of the brief closings (flickers) in the bursts due to the brief (~40 μs) lifetime of C3. Calculation of the equilibrium occupancies of the states for Scheme III E indicated that C5, the longest closed state, was occupied >98.6% of the time for the unliganded channel over the range of examined voltages of up to +70 mV.

To examine whether Scheme III E could describe the voltage dependence of the single-channel data for unliganded gating, predicted dwell-time distributions were obtained by simulating single-channel data with E for different voltages for comparison to the experimental distributions. The simulated single-channel currents were analyzed just like the experimental currents to obtain the predicted dwell-time distributions. Analyzing simulated single-channel data with filtering and noise equivalent to that in the experimental data automatically accounts for the effects of filtering (missed events) and noise on the predicted distributions.

The predicted distributions (thick lines) for the representative experiments in Fig. 6 show that Scheme III E could approximate the observed shift in the open and closed dwell-time distributions with voltage for the unliganded channel. For the experiment in Fig. 6, A–D, depolarizing from +30 to +70 mV with 0.0003 μM Ca^{2+}_i increased P_o 33-fold (from 0.000036 to 0.0012) by shifting the open intervals towards longer durations and the longer closed intervals towards briefer durations (○). A similar shift was seen for an experiment at 0.03 μM Ca^{2+}_i in Fig. 6, E–H. The distributions predicted by Scheme III E (thick lines) captured the major aspects of the single-channel data as well as the voltage-dependent shifts in the distributions, with the predictions typically falling within the scatter in the data resulting from the limited number of intervals that could be collected at the low P_os. In spite of its relative success, Scheme III E underpredicted the intermediate duration (1–10 ms) closed intervals at +30 mV for the experiment in Fig. 6, A–D. It is perhaps not surprising that Scheme III E with five states only approximated the data, as this scheme is simplified from the 10-state model expected for gating in zero Ca^{2+}_i described by the left-most subscheme of Scheme I.

Identifying the Voltage-dependent Transitions within the Subscheme of Fully Liganded States

Having identified the possible voltage-dependent transitions among the unliganded states in Scheme II, we next used the same approach to identify the voltage-dependent transitions among the fully liganded states (the right-most subscheme) in Scheme II. We have previously shown for normal mode gating and $Ca^{2+}_i \geq$ 1,000 μM, that the channel would be expected to spend >99% of its time in the fully liganded states (Rothberg and Magleby, 1999). On this basis, the rate constants and voltage dependence for transitions among the fully liganded states in Scheme II were estimated by fitting Scheme III, A–E, to 2-D dwell-time distributions ob-

TABLE II

Rate Constants for Scheme III E at +30 mV

	Unliganded*		Fully liganded‡	
	Rate constant	F/B§	Rate constant	F/B§
	s^{-1}		s^{-1}	
$k(5,4)$	1.90 ± 0.45	0.0003	640 ± 250	2
$k(4,5)$	7000 ± 750		280 ± 100	
$k(4,3)$	290 ± 290	0.05	2100 ± 1100	2
$k(3,4)$	6000 ± 6000		1300 ± 1000	
$k(4,2)$	1500 ± 550	0.2	1200 ± 810	0.6
$k(2,4)$	8700 ± 1700		1900 ± 720	
$k(3,1)$	21000 ± 3300	10	20000 ± 6000	40
$k(1,3)$	2200 ± 210		450 ± 95	
$k(2,1)$	3000 ± 2000	1	1500 ± 1400	20
$k(1,2)$	2500 ± 1300		70 ± 70	
Partial charge (e_o)‖				
q_1	+0.45 ± 0.19		+0.21 ± 0.12	
q_2	−0.39 ± 0.04		−0.54 ± 0.19	
q_3	+0.20 ± 0.25		−0.064 ± 0.09	
q_4	−0.17 ± 0.07		−0.30 ± 0.06	

*$Ca^{2+}_i \leq 0.03$ μM, channel B15 at 0.03 μM, and channel B14 at 0.03 μM, and also 0.0003 μM. ‡Ca^{2+}_i = 1,024 μM, channels B07, B14, and B16. Estimates of rate constants and partial charges are listed as mean ± SEM. §F/B is the mean forward rate constant (towards O_1) divided by the mean backward rate constant (towards C_5), and would be equivalent to the equilibrium constant for a model with only two states. ‖Partial charges for unliganded versus fully liganded channels were not significantly different.

tained with 1,024 μM Ca^{2+}_i at three to four different voltages, typically ranging from −80 to +30 mV.

As with the data obtained at very low Ca^{2+}_i, the rate constants and their voltage dependence was estimated for Scheme III, A–E. Table I (right) presents the NLR_1 and the rankings of the various schemes for three different channels studied at high Ca^{2+}_i in the fully liganded state. As was the case for the unliganded channel, Scheme III A, in which the voltage-dependent transitions were confined only to the opening and closing transitions, gave the worst descriptions of the data (lowest values of the log-likelihood and NLR_1) and also ranked the lowest, while E, in which all the transitions were voltage dependent, gave the best descriptions of the data and also ranked first among the five models.

The mean ± SEM of the estimated rate constants and their voltage dependence for Scheme III E with all states fully liganded (1,024 μM Ca^{2+}_i) are shown in Table II. As was the case for fitting the unliganded channel, a number of the rate constants were poorly defined, as reflected in the large SEM for those estimates.

The predicted distributions (thick lines) for the representative experiment in Fig. 7 shows that Scheme III E could approximate the major effects of voltage on the open and closed dwell-time distributions for the fully liganded channel for voltages ranging from −80 to +30 mV, which increased the observed P_o 37-fold, from 0.026 to 0.96. The predicted distributions described the pronounced depolarization-induced shifts in the open intervals to longer durations and in the closed intervals to briefer durations. The predicted increase in P_o from 0.022 to 0.97 was similar to the observed increase. While Scheme III E captured the major features of the single-channel data over this large range of P_o, it clearly had some deficiencies, as evident in the differences between the observed and predicted distributions and NLR_1 values of ∼0.97 (Table I), 3% less than the best possible description of 1.0.

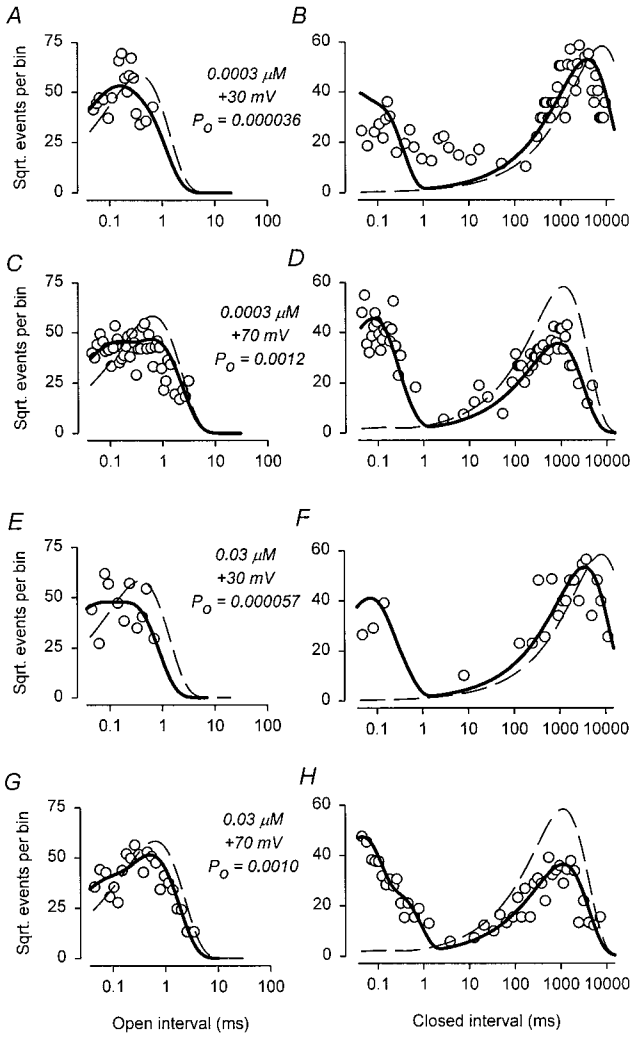

Figure 6. Dwell-time distributions at very low Ca^{2+}_i. Open and closed dwell-time distributions for 0.0003 μM Ca^{2+}_i at +30 mV (A and B) and +70 mV (C and D), and for 0.03 μM Ca^{2+}_i at +30 mV (E and F) and +70 mV (G and H). Thick solid lines are the predicted dwell-time distributions from Scheme III E. Dashed lines are the predicted dwell-time distributions from the 10-state allosteric scheme in Table I from Horrigan et al. (1999), using the rate constants denoted as Case A. The model in Table I from Horrigan et al. (1999) underpredicts the numbers of experimentally observed brief closed intervals. The numbers of fitted intervals in the distributions were: A, 36; B, 111; C, 159; D, 158; E, 38; F, 58; G, 334; and H, 298;. Channel B14.

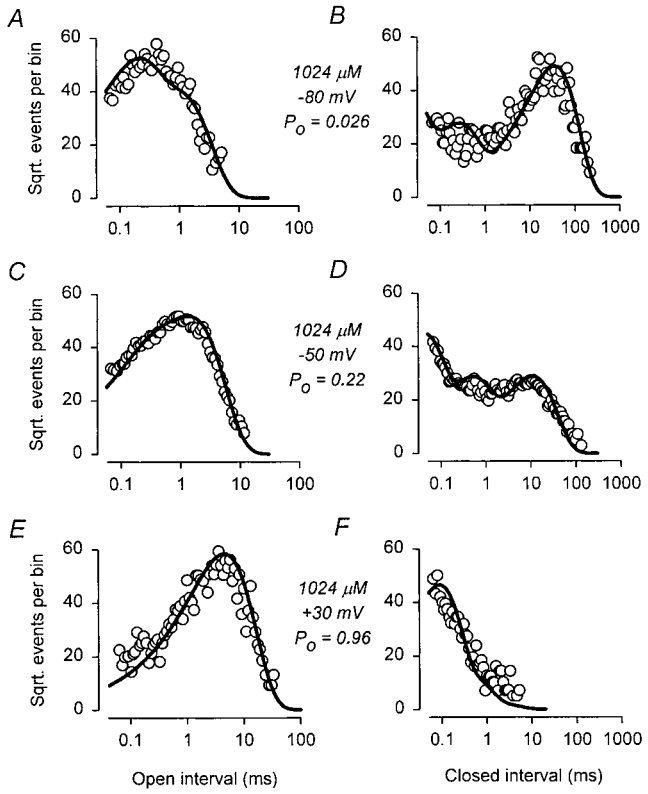

Figure 7. Dwell-time distributions at very high (1,024 μM) Ca^{2+}_i. Open and closed dwell-time distributions at −80 mV (A and B), −50 mV (C and D) and +30 mV (E and F). Thick solid lines are the predicted dwell-time distributions from Scheme III E. The numbers of fitted intervals in the distributions were: A, 550; B, 514; C, 5,139; D, 3,936; E, 1,113; and F, 647. Channel B16.

As with the unliganded channel, it is perhaps not surprising that the five-state Scheme IIIE only approximated the fully liganded gating, as this scheme is simplified from the minimal 10-state model expected for gating in the fully liganded states, as described by the right-most subscheme of Scheme I. To determine how much improvement the 10-state model might provide, we also examined the ability of a 10-state model with q constrained similar to that in Scheme III E to describe the data. The description with the 10-state model was significantly improved over Scheme III E ($P < 0.001$), with an average NLR_1 of 0.985 for the three data sets, indicating a 50% reduction in the error compared with the five-state model. While the 10-state model gave a better description of the data, so many of the large numbers of parameters were poorly defined that the focus in the present paper will be on the simpler models.

Comparison of Gating of the Unliganded and Fully Liganded Channel at +30 mV

Increasing Ca^{2+}_i from ~0 to 1,024 μM increased P_o ~20,000-fold, from ~0.00005 for the unliganded channel to 0.96 for the fully liganded channel (Figs. 6 and 7). In the context of Scheme III E, the Ca^{2+}-induced changes in gating that give this phenomenal increase in P_o can be seen in Table II, which presents each rate constant and also the ratios of the forward to backward rate constants (F/B) for each of the transitions for both the unliganded and fully liganded channels. The binding of four Ca^{2+} altered the rate constants to have three major effects: (a) the duration of the long closed state C5 was greatly decreased, (b) the duration of the long open state O1 was increased, and (c) the ratios of the forward to backward rate constants were changed to drive the gating away from the long closed state and towards the long open state.

The mean lifetime of the long closed state C5 at +30 mV was 530 ms for unliganded gating, compared with 1.6 ms for fully liganded gating, for a 330-fold increase in the rate of leaving C5 after binding four Ca^{2+} ($P < 0.001$, t test), and the mean lifetime of the long open state O1 at +30 mV was 210 μs in the unliganded state and 1.9 ms in the fully liganded state, for a ninefold decrease in the rate of leaving O1 after binding four Ca^{2+} ($P < 0.05$, t test). In addition, the binding of four Ca^{2+}_i decreased the transition rate from C4 to C5, from 7,000/s to 280/s ($P < 0.001$). This 25-fold decrease acts to increase the duration of the bursts in the fully liganded channel by slowing the return to the long closed state C5 that is the main contributor to the gaps between bursts. These Ca^{2+}-induced changes in the transition rates between C5 and C4 biased the ratio of the forward to backward rate constants (F/B) between these states, from 0.0003 for the unliganded channel to 2.0 for the fully liganded channel, for a 6,600-fold increase in the ratio for transitions towards the long open state. As another example, the Ca^{2+}-induced changes in the transition rates between O2 and O1 biased the ratio of the forward to backward rate constants between these states from 1 for the unliganded channel to 20 for the fully liganded channel, for a 20-fold increase in the ratio for transitions towards the long open state. Thus, the binding of Ca^{2+} to its allosteric sites on the BK channel acts to greatly decrease the stability of the long closed state while increasing the stability of the long open state.

In comparison with the orders of magnitude differences in some of the rate constants between the unliganded and fully liganded channels for Scheme III E, the estimates of the partial charges q_1–q_4 that convey the voltage sensitivity to specific transitions (see Eq. 3) were typically within a factor of two between the unliganded and fully liganded channel (Table II), and none of the differences were significant ($P > 0.2$–0.5). The lack of significant effect of Ca^{2+}_i on estimates of the partial charge is consistent with the apparent lack of effect of Ca^{2+}_i on the apparent limiting slopes of the plots of P_o versus membrane potential observed in Fig. 2 B. Nevertheless, due to the variability in the estimates of partial

charge among channels, a small effect of Ca^{2+} on partial charge cannot be excluded, as observed by Cui et al. (1997) from Boltzmann fits to macroscopic currents.

Scheme II Describes the Voltage and Ca^{2+}_i Dependence of the Gating

The results in the previous two sections identified the voltage-dependent steps in the gating of the unliganded and fully liganded channel as being consistent with Scheme III E. With this information, it was possible to examine whether Scheme II could account simultaneously for the voltage and Ca^{2+}_i dependence of the gating. In carrying out this test, it was assumed that the voltage-dependent steps for the partially liganded channel were also consistent with Scheme III E, and it was further assumed that the Ca^{2+}-binding and -unbinding rate constants were independent of voltage, since there was no evidence to the contrary. With these assumptions, the rate constants for Scheme II were estimated by simultaneous fitting 2-D dwell-time distributions obtained over a range of voltages and Ca^{2+}_i. The data for the fitting were obtained at five to six different voltages and three to four different Ca^{2+}_i for each of three different channels, giving 6–10 2-D dwell-time distributions that were simultaneously fitted for each of the channels. For channel B13, the voltage ranged from −40 to +50 mV and the Ca^{2+}_i ranged from 5.5 to 20.3 μM. For channel B14, the voltage ranged from −40 to +70 mV and the Ca^{2+}_i ranged from 0.0003 to 1,024 μM and, for channel B16, the voltage ranged from −50 to +40 mV and the Ca^{2+}_i ranged from 20.3 to 1,024 μM. For channels B13 and B16, data were not obtained at ∼0 Ca^{2+}_i, so the rate constants for the transitions among the unliganded states were set to the mean values in Table II (left), determined from the separate fitting of data obtained at ≤0.03 μM Ca^{2+}_i. Setting the values of the rate constants of the unliganded states (vs. letting them be free parameters) had little effect on the estimates of the other rate constants in Scheme II for these channels. Although the constraints on the voltage-dependent steps were given by Scheme III E during the fitting, the specific partial charge estimates q_1–q_4 were free parameters.

Estimates of the most likely rate constants for Scheme II for channel B13 are presented in Table III, together with estimates of q_1–q_4 for channels B13, B14, and B16. Also presented in Table III are the approximate ratios of the rate constants for the various transitions pathways between states for those transitions in which both rate constants were >0.1 s^{-1}. These estimates were obtained from the means of the rate constants for channels B13, B14, and B16. F/B in Table III gives the ratio of the forward (towards O1) to the backward (towards C15) rate constants for those transition pathways independent of agonist binding or unbinding, and would be equivalent to the equilibrium constant for a model with only two states. In general, the ratios of the forward to backward rate constants (F/B) increase as the number of bound Ca^{2+} increase. B/F gives the ratios of the backward (towards C15) to the forward (towards O1) rate constants for the agonist-dependent transitions, and would be equivalent to the dissociation constant for a model with only two states. Since the forward agonist-dependent rate constants have units of $\mu M^{-1}\,s^{-1}$, the ratio B/F has units of μM, corresponding to the concentration at which the individual forward rate constant is equal to its corresponding backward rate constant.

To examine whether Scheme II with the most likely rate constants could simultaneously describe the Ca^{2+} and voltage dependence of the single-channel data, predicted dwell-time distributions were obtained by simulating and then analyzing the simulated single-channel data. Results are shown in Fig. 8 for channel B13, where the predicted distributions (thick lines) gave a reasonable description of the observed open and closed dwell-time distributions obtained over a 134-fold change in P_o, from 0.0061 to 0.82, for voltages ranging from −40 to +50 mV, and for three Ca^{2+}_i of 5.5, 12.3, and 20.3 mM. The voltage- and Ca^{2+}-dependent shifts in the distributions were predicted with a single set of parameters (Table III). A similar agreement between experimental and predicted results was observed for the two other examined channels using seperately determined sets of rate constants for each channel.

The ability of Scheme II to give a reasonable description of the voltage and Ca^{2+} dependence of the single-channel kinetics in Fig. 8 is reflected in an NLR_1 value of 0.987, and the NLR_1 values of 0.983 and 0.987 for the other two channels (B16 and B14, respectively) examined in this manner. Although these values are less than the theoretical best description of 1.0, they do indicate an average likelihood difference of only ∼1.4% per interval pair between the theoretical best description and that predicted by Scheme II. A less than ideal description would be expected, since Scheme II is simplified from the more complete gating mechanism described by Scheme I.

To examine whether Scheme II could describe the effects of Ca^{2+}_i on P_o, $V_{1/2}$, and q_{eff} over an even wider range of Ca^{2+}_i, Scheme II with the most likely parameters for each of three channels was used to predict P_o versus voltage curves for values of Ca^{2+}_i ranging from 0.0003 to 1,024 μM. The P_o versus voltage curves were also used to estimate the values of $V_{1/2}$ and q_{eff} over a range of Ca^{2+}_i for the three channels. The predicted values of P_o, $V_{1/2}$, and q_{eff} were plotted in Fig. 2 A–D as continuous (channel B13), dashed (channel B14), and dotted (channel B16) thin lines. The points on these figures are a composite of data from a number of different

TABLE III

Rate Constants from Scheme II at +30 mV for Channel B13

Ca^{2+} binding		Ca^{2+} unbinding		B/F*	O-O forward		O-O backward		F/B‡
k	$\mu M^{-1}\,s^{-1}$	*k*	s^{-1}	μM	*k*	s^{-1}	*k*	s^{-1}	
15, 14	22	14, 15	5000	200	10, 5	3000	5, 10	2500	1
14, 13	800	13, 14	25000	80	9, 4	3900	4, 9	20000	0.5
13, 12	130	12, 13	190	100	8, 3	3200	3, 8	2600	2
12, 11	40	11, 12	6600	50	7, 2	<0.1	2, 7	<0.1	6
5, 4	<0.1	4, 5	<0.1	—	6, 1	3300	1, 6	800	20
4, 3	<0.1	3, 4	<0.1	—					
3, 2	<0.1	2, 3	<0.1	—					
2, 1	140	1, 2	150	3					

C-O		O-C		F/B‡	C-C forward		C-C backward		F/B‡
k	s^{-1}	*k*	s^{-1}		*k*	s^{-1}	*k*	s^{-1}	
20, 10	1500	10, 20	8700	0.2	15, 20	1.9	20, 15	7000	0.0002
19, 9	13000	9, 19	1000	6	14, 19	190	19, 14	7500	0.04
18, 8	45000	8, 18	15000	4	13, 18	3300	18, 13	25000	0.3
17, 7	45000	7, 17	18000	2	12, 17	<0.1	17, 12	<0.1	—
16, 6	2900	6, 16	2600	5	11, 16	25000	16, 11	5600	4
25, 5	21000	5, 25	2200	10	20, 25	130	25, 20	6000	0.02
24, 4	850	4, 24	<0.1	20	19, 24	<0.1	24, 19	14000	—
23, 3	1100	3, 23	510	10	18, 23	<0.1	23, 18	<0.1	0.2
22, 2	6900	2, 22	1700	2	17, 22	<0.1	22, 17	<0.1	2
21, 1	23000	1, 21	480	60	16, 21	<0.1	21, 16	<0.1	—

Partial Charge Estimates from Scheme II for Channels B13, B14, and B16

	B13 (e_o)	B14 (e_o)	B16 (e_o)	Mean ± SEM (e_o)
q_1	+1.6	+0.97	+0.58	+1.05 ± 0.30
q_2	−0.19	−0.26	−0.63	−0.36 ± 0.21
q_3	−0.30	+0.14	+0.01	−0.05 ± 0.13
q_4	−0.072	+0.12	−0.24	−0.06 ± 0.10

*B/F is the mean of the average backward rate constant (towards C15) divided by the mean of the average forward rate constant (towards O_1) for channels B13, B14, and B16, and would be equivalent to the dissociation constant for a model with only two states. ‡F/B is the mean of the average forward rate constant divided by the mean of the average backward rate constant for channels B13, B14, and B16, and would be equivalent to the equilibrium constant for a model with only two states. Estimates of the SEM for the B/F and F/B values were typically similar in magnitude to the indicated means of these values.

channels so an exact fit would not be expected. Nonetheless, the results show that Scheme II approximated both the P_o vs. voltage curves and the effective gating charge for the three channels (Fig. 2, A–C), and also the general shape of the Ca^{2+}-dependent and -independent regions of the $V_{1/2}$ versus $Ca^{2+}{}_i$ relation for two of the three channels (Fig. 2 D). Scheme II also approximated the general effects of voltage on the mean open and closed interval durations (Fig. 3, A and B, thin lines) and also the effect of voltage on the apparent mean opening and closing rates (Fig. 3 D, thin lines).

Scheme II predicted single-channel current records that were essentially indistinguishable from the experimental data over wide ranges of $Ca^{2+}{}_i$ and voltage, after allowing for stochastic variation and a slightly more stable baseline in the simulated data. Examples of simulated current records can be found in the online supplement to this paper for comparison with the experimental data in Fig. 1.

The partial charges q_1–q_4 in Table III show that, in terms of Scheme II, the gating steps with the most voltage dependence were the transitions between the closed states (closed–closed) and between the open states (open–open) in each of the five parallel subschemes (as described by Scheme III E) that form Scheme II. For all three channels, depolarization facilitated the forward steps (mean $q_1 = +1.05\ e_o$) and slowed the backwards steps (mean $q_2 = -0.36\ e_o$). The closed–open transitions (mean $q_3 = -0.05$) and the open–closed transitions (mean $q_4 = -0.06$) were much less voltage sensitive, with the variability in the estimates exceeding the mean values.

Although there was reasonable consistency among the partial charge estimates for the three different channels, for many of the rate constants there was considerable variability among estimates for the three different channels, as many of the rate constants were poorly defined. Consequently, the rate constants in Table III must be viewed as an example of a set of most likely rate constants that, when used with Scheme II,

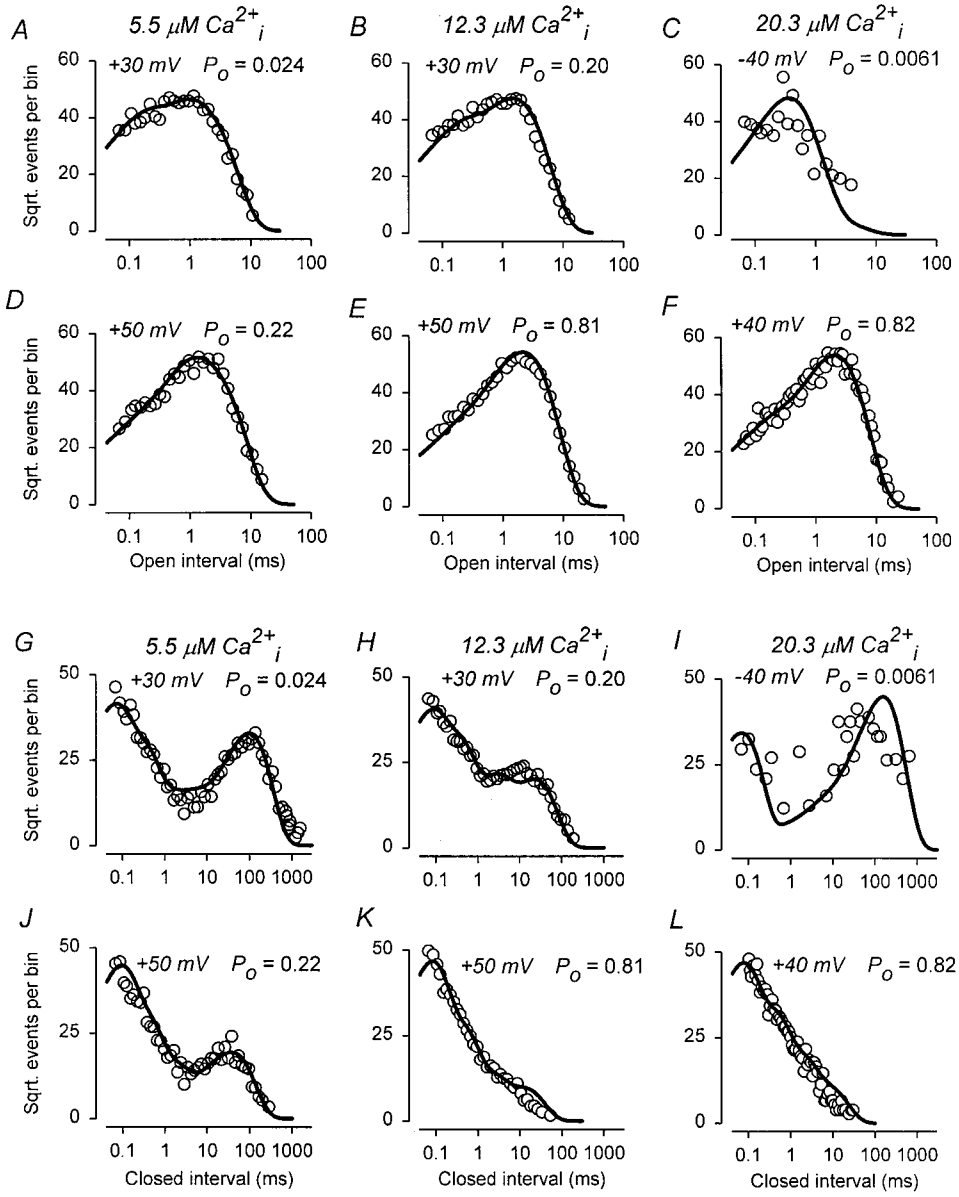

Figure 8. Dwell-time distributions over a range of voltage and Ca^{2+}_i. Thick solid lines are the predicted dwell-time distributions from Scheme II using the rate constants and partial charge estimates given in Table III. The numbers of fitted intervals in the distributions were: C, 90; F, 5,330; I, 93; and L, 3,820; and the same as in Fig. 4 for the remaining distributions. Channel B13.

can describe the gating of the channel without placing too much emphasis on the specific values. The most likely rate constants for the various channels were sufficient to show that Scheme II could describe the gating, even though they do not necessarily represent unique values of the rate constants.

Partial Charge Estimates

In the above sections, estimates of the partial charge movement associated with specific gating steps for Scheme II were obtained separately under the three conditions of ~0 Ca^{2+}_i, saturating Ca^{2+}_i, and for simultaneously fitting data over a wide range of Ca^{2+}_i. The mean ± SEM of these estimates are presented in Table IV. The partial charge estimates for the forward (q_1 = +0.57 e_o) and backward (q_2 = −0.43 e_o) steps for the C-C and O-O transitions in Scheme III E were significantly different from zero ($P < 0.05$, signs test). The estimates for the C-O transitions (q_3 = +0.030) were not significantly different from zero ($P > 0.4$), and the estimates for the O-C transitions (q_4 = −0.18) were significantly different from zero ($P < 0.05$). These mean global estimates suggest that the voltage dependence of the gating arises primarily from the C-C and O-O transitions in each subscheme (Scheme III E), with less voltage dependence arising from the opening C-O and closing O-C transitions. These findings, obtained from the simultaneous analysis of single-channel data recorded over a range of both voltage and Ca^{2+}_i, are consistent with findings obtained from analysis of macro-

TABLE IV

*Means of All Partial Charge Estimates for Schemes II and III E**

Gating step‡		Partial charge (e_o)
Forward O-O and C-C transitions	q_1	$+0.57 \pm 0.16$§
Reverse O-O and C-C transitions	q_2	-0.43 ± 0.07§
C-O transitions	q_3	$+0.03 \pm 0.10$
O-C transitions	q_4	-0.18 ± 0.05§

*Means ± SEM were determined from nine independent estimates of partial charges using Scheme III E for unliganded ($n = 3$) and fully liganded ($n = 3$) channels over a range of voltages, and Scheme II for simultaneous fitting of data obtained over a range of Ca^{2+}_i and voltages ($n = 3$). ‡q's are subscripted corresponding to Scheme III E. §Significantly different from zero ($P < 0.05$, signs test).

scopic ionic and gating currents obtained over a wide range of voltage at ~0 Ca^{2+}_i (Horrigan et al., 1999; Horrigan and Aldrich, 1999).

Voltage-induced Shifts in the Gating

We have previously described, in terms of a two-tiered model such as Scheme II, how increased Ca^{2+} shifted the gating from the closed states in the top left of the scheme to the open states in the bottom right (Figure 14 in Rothberg and Magleby, 1999). Fig. 9 presents the same type of information for the voltage-induced shift in gating. Depolarizing from −40 to +40 mV (at a fixed Ca^{2+}_i of 20.3 μM) also shifted the gating from the closed states in the top left of the two-tiered Scheme II to the open states in the bottom right. At −40 mV (P_o = 0.0061), the channel spent 48% of its time in the top left–most closed state C15 (Fig. 9 A) and only 0.01% in the bottom right–most open state O1. In contrast, at +40 mV (P_o = 0.82), the channel now spent only 7.7% of its time in the top left–most closed state C15 and 61% of its time in the bottom right–most open state O1 (Fig. 9 D). This shift in equilibrium occupancy with depolarization results mainly from a decreased frequency of entry into the longer closed states and an increased frequency of entry into the longer open states (Fig. 9, C and F), and less from changes in the lifetimes of the states (Fig. 9, B and E). (When examining Fig. 9, keep in mind that small changes in the amplitudes of the bars can have large effects on the parameters because of the logarithmic coordinates.)

DISCUSSION

Two-Tiered Gating Mechanisms Can Describe the Gating of BK Channels Over Wide Ranges of Voltage, Ca^{2+}, and P_o

This study used single-channel analysis to examine the mechanism of the voltage- and Ca^{2+}-dependent gating of native BK channels from cultured rat skeletal muscle. It was found that the simplified two-tiered model, Scheme II, could describe the major effects of voltage and Ca^{2+}_i and their interaction on the single-channel kinetics during normal activity over wide ranges of voltage (−80 to +80 mV), Ca^{2+}_I (~0 to 1 mM), and P_o (~10^{-4} to 0.96), as shown in Figs. 2 and 6–8. Since Scheme II is simplified from Scheme I, it would be expected that the full two-tiered model described by Scheme I would give even better descriptions of the data, since Scheme I reflects more completely the subunit structure of the channel. In Scheme I, the top and bottom tiers contain the closed and open states of the channel, respectively. The 25 states on each tier arise because each of the four subunits can bind Ca^{2+} (indicated by shading) and also make voltage-dependent transitions between two conformations (indicated by squares and circles).

The two-tiered gating mechanism of Scheme I can be functionally divided into five parallel (two-tiered) subschemes, each having five closed and five open states. The subschemes differ only in the numbers of Ca^{2+} bound to each, with zero, one, two, three, or four bound Ca^{2+}. The binding and unbinding of Ca^{2+} shifts the channel laterally between the parallel subschemes, while voltage shifts the gating among the 10 states within each of the subschemes, including between the upper and lower tiers. Both Ca^{2+} binding and depolarization increase P_o by increasing the stability of the open states. The Ca^{2+}-induced increase in stability is illustrated in Rothberg and Magleby (1999; Figure 14, A and D), where increasing Ca^{2+}_i from 5.5 to 1,024 μM Ca^{2+}_i increased the equilibrium occupancy of the open states from 0.06 to 0.97 at + 30 mV. The depolarization-induced increase in stability is illustrated in Fig. 9, A and D, where depolarization from −40 to +40 mV increased the equilibrium occupancy of the open states from 0.0061 to 0.82 in 20.3 μM Ca^{2+}_i.

Depolarization increases P_o by increasing the rate of the (forward) conformational changes of the subunits and decreasing the rate of the backward conformational changes of the subunits (Scheme I, oblique arrow), and this is the case for both the closed–closed transitions on the top tier and the open–open transitions on the bottom tier (Scheme III E and Tables II–IV). Depolarization also alters the transition rates between the two tiers to stabilize the open states (vertical arrow). These effects of voltage obtained from ~0 to saturating Ca^{2+}_i in our study are consistent with those of Horrigan et al. (1999) and Horrigan and Aldrich (1999) obtained at ~0 Ca^{2+}_i.

MWC- and Eigen-type Models Are Subsets of Scheme I

Before considering Scheme I as a working hypothesis, it is necessary to establish that simpler models do not describe all of the experimental observations. Most previous studies of the gating of BK channels have been based on either Eigen (1968)-type models or one of two different forms of the MWC model (Monod et al.,

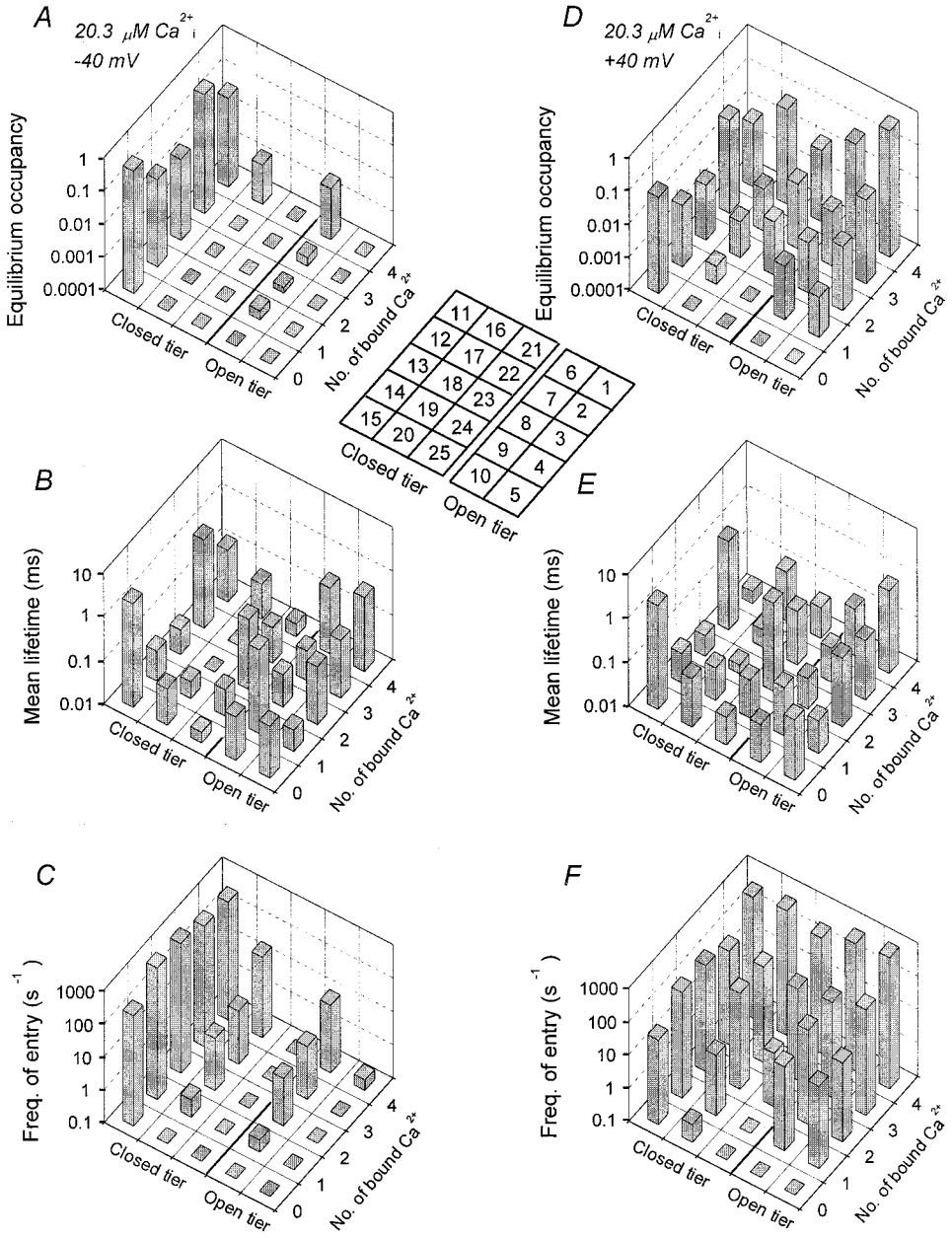

Figure 9. Voltage-dependent shifts in gating according to Scheme II. (Inset) Numbers relate the state numbers in Scheme II to the states in the various plots. (A and D) Predicted equilibrium state occupancies at 20.3 μM Ca^{2+}_i at −40 and +40 mV, respectively. (B and E) Mean lifetimes of the states at −40 and +40 mV, respectively. (C and F) Frequency of entry into each state at −40 and +40 mV, respectively. Channel B13.

1965), or extensions of these models (e.g., Magleby and Pallotta, 1983; McManus and Magleby, 1991; DiChiara and Reinhart, 1995; Wu et al., 1995; Cox et al., 1997; Cui et al., 1997; Rothberg and Magleby, 1998 Horrigan et al., 1999; Horrigan and Aldrich, 1999). MWC models with Ca^{2+} as the allosteric activator predict that no intermediate or secondary states should be entered during the gating at intermediate levels of Ca^{2+}_i. Yet gating in such states is observed (Ferguson et al., 1993; Rothberg and Magleby, 1998). MWC and Eigen models with Ca^{2+}_i as the allosteric activator also predict that gating will occur in fewer states at the extremes of both ~0 Ca^{2+}_i (Horrigan et al., 1999; Horrigan and Aldrich, 1999; Nimigean and Magleby, 2000; Talukder and Aldrich, 2000) and saturating Ca^{2+}_i (Rothberg and Magleby, 1999) than are observed experimentally. Such models also predict that there would be no correlation among adjacent interval durations in single-channel recordings at the extremes of both ~0 and saturating Ca^{2+}_i, in contrast to the correlations that are observed (Nimigean et al., 1999; Rothberg and Magleby, 1999). Ionic and gating currents obtained in the absence of Ca^{2+}_i, but over a wide range of voltage, are inconsistent with the form of the MWC model in which Ca^{2+}_i is the allosteric activator, but are consistent with an MWC-type model in which voltage is the allosteric activator (Horrigan et al., 1999; Horrigan and Aldrich, 1999), but an MWC model with voltage as

the allosteric activator cannot then account for the effects of Ca^{2+}_i. Taken together, then, these observations indicate that the MWC- and Eigen-type models are too simple to describe the gating of BK channels over a wide range of both voltage and Ca^{2+}_i.

Nevertheless, MWC- and Eigen-type models can describe many features of the gating over restricted conditions. The reason for this is that these models are contained within the two-tiered 50-state model, where both Ca^{2+} and voltage are separate allosteric activators. Restricting the experimental conditions can effectively reduce the 50-state model to one of the simpler models, so that under restricted conditions, the gating can be well approximated by these simpler models. Thus, the two-tiered 50-state model is a unifying model, as it includes and expands upon the previous models for the gating of BK channels.

Additional Evidence for Two-Tiered Gating Mechanisms

Scheme I indicates that up to four Ca^{2+} can be bound. Evidence for three to four bound Ca^{2+} for maximal activation comes from Hill coefficients typically approaching three to four for plots of P_o vs. Ca^{2+}_i (McManus and Magleby, 1991; Cox et al., 1997; Rothberg and Magleby, 1999; and extensive references contained in these references).

Scheme I indicates that the channel can gate among as many as five open and five closed states in both 0 Ca^{2+}_i (left-most subscheme) and saturating Ca^{2+}_i (right-most subscheme). The gating at ~0 Ca^{2+}_i is consistent with the left-most subscheme in Scheme I with no bound Ca^{2+} (Horrigan et al., 1999; Horrigan and Aldrich, 1999; and Fig. 6 for reduced Scheme III E), and the gating in saturating Ca^{2+}_i is consistent with the right-most subscheme in Scheme I with four Ca^{2+} bound to each state (Rothberg and Magleby, 1999; and Fig. 7 for reduced Scheme III E). It follows immediately, then, that the gating with one, two, or three bound Ca^{2+} would require three additional subschemes located between the subschemes for gating with zero and four bound Ca^{2+}, consistent with Scheme I.

Scheme I has a tier of closed states and a tier of open states because there is an additional conformational change associated with the opening–closing transitions that is separate from the conformational changes of the four voltage-sensing subunits. Evidence for this additional conformational change in BK channels at ~0 Ca^{2+}_i has been obtained with voltage-jump studies of ionic and gating currents (Horrigan et al., 1999; Horrigan and Aldrich, 1999). More complex models for the gating of voltage-activated K^+ channels also include such concerted conformational changes (Zagotta et al., 1994; Roux et al., 1998; Schoppa and Sigworth, 1998). It should be noted that the idea of a separation of the conformational changes of the voltage sensors from that of the opening–closing transition, as in Scheme I, is not new, but has been considered previously for Ca^{2+} channels (Marks and Jones, 1992), *Shaker* K^+ channels (McCormack et al., 1994), and the Ca^{2+} release channel in muscle (Ríos et al., 1993).

Scheme I has five open states connected to five closed states, giving five separate pathways in each subscheme between the open and closed states in the two tiers. Thus, at least five separate transition pathways between the open and closed states are available over the entire range of Ca^{2+}_i. Support for gating with multiple separate transition pathways over the entire range of Ca^{2+}_i comes from observations of correlation between adjacent open and closed intervals for single-channel data obtained from ~0 to saturating Ca^{2+}_i (~0 Ca^{2+}_i, Nimigean et al., 1999; intermediate Ca^{2+}, McManus et al., 1985; McManus and Magleby, 1991; Rothberg and Magleby, 1998; saturating Ca^{2+}, Rothberg and Magleby, 1999).

In Scheme I, the voltage-dependent steps are separate from the Ca^{2+}-dependent steps. Support for separate steps comes from the observations that voltage still activates the channel in ~0 Ca^{2+} and that changes in Ca^{2+}_i at very low Ca^{2+}_i have little effect on the gating (Figs. 1, 2, and 6; Meera et al., 1996; Rothberg and Magleby, 1996; Stefani et al., 1997; Cui et al., 1997; Horrigan and Aldrich, 1999). Support that voltage does not act solely through changing the effective Ca^{2+}_i at the binding sites is our observation that voltage and Ca^{2+}_i have differential effects on the kinetics of the gating (Fig. 4). Ca^{2+}_i also is not required to serve as the effective gating charge by binding to some titratable site (Stefani et al., 1997), as the observed maximum voltage dependence obtained from limiting slope measurements was little affected when Ca^{2+}_i was changed from ~0 to 1 mM in our experiments (Fig. 2, B and C), although we cannot rule out that there is some effect (Cui et al., 1997). Detailed kinetic studies on macroscopic ionic currents also argue for at least one voltage step that is separate from Ca^{2+} binding (Cui et al., 1997).

Scheme I predicts that gating charge movement can occur after the channel opens its pore through transitions among the open states on the bottom tier. Support for this prediction comes from the observations of charge movement after the channel opens (Stefani et al., 1997; Horrigan and Aldrich, 1999).

Thus, support for Scheme I comes from both its ability to describe the single-channel kinetics over wide ranges of voltage, Ca^{2+}_i, and P_o, and also from the additional experimental observations discussed in this section that lend support to the underlying assumptions embodied in Scheme I.

Gating Charge and the Voltage-dependent Steps

The effective gating charge for activation of the BK channels by voltage, estimated from the maximum limiting slope of plots of P_o vs. voltage, was 2.3 ± 0.6 e_o (Fig. 2),

and this effective gating charge was predicted by Scheme II (Fig. 2 C). Our estimate of effective gating charge compares favorably with estimates of 1.1–1.8 e_o obtained from *mSlo* by Cui et al. (1997), 1.6 ± 0.2 e_o obtained from *hSlo* by Diaz et al. (1998), and of 2.0 e_o obtained from *mSlo* by Horrigan et al. (1999). Interestingly, Horrigan et al. (1999) found that the limiting slope becomes more shallow for P_os $< 10^{-4}$ at $\sim$0 Ca^{2+}_i. Calculations with Scheme II using the rate constants in Table III indicated an approximately twofold decrease in limiting slope for P_os $<$ 10^{-4} and $Ca^{2+}_i < 1$ μM (not shown). Thus, the two-tiered scheme can predict the mean effective gating charge and also a decrease in limiting slope at very low P_o.

In the context of Schemes I and II, the effective gating charge arises from voltage-dependent conformational changes. Our mean estimates of partial charge movement associated with the forward (q_1) and backward (q_2) steps for both C-C and O-O transitions in Scheme III E were +0.57 e_o for q_1 and −0.43 e_o for q_2 (Table IV). These estimates can be compared with those of +0.27 e_o and −0.27 e_o obtained by Horrigan and Aldrich (1999) at $\sim$0 Ca^{2+}_i for a model given by the left-most subscheme in Scheme I, where no Ca^{2+} are bound. There is reasonable agreement between our estimates and those of Horrigan and Aldrich (1999) when it is considered that our simplified Scheme III E has only two forward and two backward transitions (as if two subunits were moving simultaneously for each transition) compared with the four forward and four backward transitions in their scheme. Thus the summed partial charges for the two forward C-C transitions for Scheme III E (+1.14 e_0) is similar to the summed partial charges for the four forward C-C transitions from Horrigan et al. (1999, Table I; +1.08 e_0), and the summed partial charges for the two backward C-C transitions for Scheme III E (−0.86 e_0) is similar to the summed partial charges for the four backward C-C transitions from Horrigan et al. (1999, Table I; −1.08 e_0). Our estimates for the partial charge movement for Scheme III E for the C-O transition q_3 (+0.03 e_o) is less than, but in the same direction as, the estimate of +0.26 obtained by Horrigan et al. (1999), and our estimate for the O-C transition of q_4 (−0.18 e_o) is similar to that of −0.14 e_o obtained by Horrigan et al. (1999). Thus, our estimates obtained over a wide range of Ca^{2+} are consistent with previous observations obtained at Ca^{2+}_i and support the hypothesis that the forward and backward C-C and O-O transitions in Scheme III E are the primary voltage-dependent steps (Scheme I, oblique arrow) with the C-O and O-C steps being less voltage dependent (vertical voltage-dependent arrow in Scheme I).

The Rate Constants for Scheme II Represent Combined Rate Constants from Scheme I

Because of the large numbers of rate constants in Scheme I, we have used the simplified Scheme II, drawn from Scheme I, to assess Scheme I. To reduce further the numbers of rate constants, we have limited the number of transition pathways between the parallel subschemes in the simplified Scheme II. Since, based on subunit structure, the channel would be expected to gate like the more complex Scheme I rather than the simplified Scheme II, the individual rate constants for the simplified scheme necessarily reflect combined rate constants from the more complex scheme. Consequently, while the rate constants for the simplified Scheme II are adequate to evaluate and rank models and to predict single-channel gating kinetics, they to not necessarily reflect a single transition rate, and should be interpreted with caution. Furthermore, even with reduced numbers of rate constants for Scheme II, many of the rate constants were not unique, being poorly defined.

In spite of these limitations, the general Ca^{2+}- and voltage-dependent shifts in the equilibrium occupancies, mean lifetimes, and frequency of entry into the various states give information about the underlying mechanism, as it is these shifts that describe the experimental data. These shifts are illustrated in Fig. 9 for the voltage dependence of the gating, and in Figure 14 in Rothberg and Magleby (1999) for the Ca^{2+} dependence of the gating.

Where Do the Flickers Come From?

A characteristic kinetic feature of the gating of BK channels is the large number of brief closed intervals (flickers) entered during normal activity (McManus and Magleby, 1988). Scheme II accounts for the flickers (as well as the longer closed intervals) over the wide ranges of voltage, Ca^{2+}_i, and P_o in our study, as it describes the closed dwell-time distributions over these conditions (Figs. 6–8, thick lines). Scheme II also gives a reasonable approximation of the mean open- and closed-intervals durations (Fig. 3), which are highly sensitive to flickers. In terms of Scheme II (and by projection, also Scheme I), the observed flickers arise from transitions between open states in the lower tier and brief lifetime closed states in the upper tier.

Horrigan and Aldrich (1999) have described the voltage-dependent gating of *mSlo* BK channels in $\sim$0 Ca^{2+} using a model described by the left-most subscheme in Scheme I, with the assumption that the rate constants for the voltage-dependent conformational changes of each of the four subunits were identical and independent of the conformational states of the other subunits. To test whether the rate constants they found could describe the steady state single channel data in $\sim$0 Ca^{2+}, we simulated single-channel currents using the rate constants in Table I, Case A of Horrigan and Aldrich (1999), and plotted the predicted dwell-time distributions as dashed lines in Fig. 6. These rate constants gave excel-

lent descriptions of their ionic and gating current data, and also came remarkably close to describing the open intervals and the component of long closed intervals in the single-channel dwell times in Fig. 6, a credit to their predictive power. However, the rate constants from Case A do not describe the brief closed intervals (flickers) observed in the single-channel data, as shown in Fig. 6 and also commented on by Talukder and Aldrich (2000).

Since the state structure of the model of Horrigan and Aldrich (1999) is the same as that of Scheme I in 0 Ca^{2+}_i, the inability of the model (with rate constants from Case A) to describe the flickers could indicate that either real differences exist between the kinetic behavior of *mSlo* and native BK channels, or, alternatively, the state structure of Scheme I may be too simple to account for both the flickers and the complex voltage dependence of the ionic and gating currents during activation and deactivation. Since previous studies have suggested that *mSlo* and native BK channels are similar in their single-channel kinetics (Figure 7 in Nimigean and Magleby, 1999), it is possible that the structure of Scheme I is yet too simple. If so, then there would have to be yet another tier of closed states in Scheme I with brief lifetimes to generate the flickers in the data. The additional tier of closed states could either be between the open and closed tiers or below the open tier, creating a multi-tiered gating mechanism. Some support for a multi-tiered gating mechanism comes from our observations on the gating of BK channels in saturating Ca^{2+}_i, where models with an additional tier of brief closed states ranked higher than models without such a tier (Rothberg and Magleby, 1999).

Scheme I Itself Is a Simplification

Schemes I and II assume that the properties of each state are determined by both the number of bound Ca^{2+} and the number of subunits that have undergone a conformational change, without regard to which specific subunits have bound Ca^{2+} and which have undergone conformational changes. If Ca^{2+} has different effects depending on whether or not it binds to subunits that have undergone a conformational change, then there would be 35 possible combinations (Eigen, 1968). If Ca^{2+} bound to diagonal or adjacent subunits confers different properties on the states and if conformational changes in diagonal and adjacent subunits also confer different properties on the states, then there would be 55 possible combinations of subunits and Ca^{2+} binding (Cox et al., 1997; Rothberg and Magleby, 1999). Recent work on other channels suggests that the positions of the subunits that have undergone conformational changes does matter. Channels formed by adjacent wild-type or mutant subunits have been found to have different properties than channels formed of alternating subunit types (Liu et al., 1996; Zheng and Sigworth, 1998). If adjacent and diagonal subunit configurations and Ca^{2+} bindings do confer different properties to the gating of BK channels, then Scheme I would have to be expanded from 25 to 55 states on each tier to include all the possible states. If an additional tier of closed states is needed for flickers, then this would add an additional 55 states.

While Scheme II can serve as a starting point to quantitatively define the interactions between the voltage- and Ca^{2+}-dependent activation of BK channels, the determined sets of rate constants for Scheme II are limited to the specific physiological state of the channel used to estimate the rate constants. The reason for this is that so many other factors alter BK channel activity, such as phosphorylation (Reinhart et al., 1991; Levitan, 1994; Bielefeldt and Jackson, 1994), redox reactions (DiChiara and Reinhart, 1997; Thuringer and Findlay, 1997), beta subunits (McManus et al., 1995; Tanaka et al., 1997; Nimigean and Magleby, 1999, 2000; Wallner et al., 1999; Xia et al., 1999; Brenner et al., 2000), modding (McManus and Magleby, 1988; Smith and Ashford, 1998), and alternative splicing (Lagrutta et al., 1994; Jones et al., 1999) that specific rate constants would have to be determined for each combination of the various factors. In addition, to account for activity in modes other than normal and also for inactivating beta subunits, additional states, perhaps in the form of additional tiers, would have to be added to Scheme I.

Are BK Channels Voltage or Calcium Activated?

In terms of Scheme I, the channel gates in 0 Ca^{2+}_i as a purely voltage-activated channel among the five closed and five open unliganded states (left-most subscheme). Ca^{2+}_i-dependent steps are not required for full activation in ~0 Ca^{2+}_i, as depolarizing voltage steps to +300 mV with ~0 Ca^{2+}_i can fully activate the channel (Horrigan et al., 1999). In saturating Ca^{2+}_i, where the channel would be gating in the right-most subscheme of Scheme I, hyperpolarizing potentials to approximately −180 mV can essentially eliminate activity (Meera et al., 1996; Cui et al., 1997). BK channels are thus voltage-activated channels that are modulated by Ca^{2+}_i (Meera et al., 1996; Cox et al., 1997; Cui et al., 1997; Stefani et al., 1997; Diaz et al., 1998). Ca^{2+}_i in the range of ~0.1–50 μM then modulates the gating by moving the voltage towards hyperpolarized potentials for half maximal activation, by changing the intrinsic closed–open equilibrium, with little effect on the voltage sensitivity (Fig. 2). The shift in equilibrium results because each additional bound Ca^{2+} leads to increases in the ratios of the forward to backward rate constants, driving the equilibrium further towards the long open state (Tables II and III). Consistent with a voltage-activated and Ca^{2+}-modulated channel, it has been suggested that BK channels may have evolved from an ancestral

voltage-sensitive K^+ channel, with the later addition of the extended COOH-terminal tail as a Ca^{2+}-dependent modulatory domain (Schreiber et al., 1999).

If the BK channel is, from a mechanistic viewpoint, voltage activated and Ca^{2+} modulated, should the "calcium activated" name of the channel be changed to reflect the underlying mechanism? We think not. Under physiological conditions, Ca^{2+}_i is usually the limiting factor controlling activation, not voltage, since voltage changes within the physiological range will not activate the channel unless Ca^{2+}_i is elevated above the typical resting level in cells. Furthermore, the voltage dependence of BK channels ($\sim$11–15 mV/e-fold change in P_o; effective charge movement of $\sim$2 e_o) is considerably less than the voltage dependence of other K^+ channels ($\sim$2 mV/e-fold change; effective charge movement of $\sim$13 e_o; Islas and Sigworth, 1999).

Conclusions

This study presents a comprehensive kinetic gating mechanism for BK channels that can describe the major features of both Ca^{2+} and voltage dependence of the single-channel kinetics over the entire range of $\sim$0 to saturating Ca^{2+}_i. The two-tiered 50-state working hypothesis both expands upon and unifies many of the previous models, which are nested within the 50-state scheme. Nevertheless, as with previously proposed mechanisms, it will undoubtedly be necessary to expand upon this mechanism to account for all details of the gating.

This work was supported in part by grants from the National Institutes of Health (NS007044 and AR32805) and the Muscular Dystrophy Association.

Submitted: 20 December 1999
Revised: 18 May 2000
Accepted: 22 May 2000

REFERENCES

Adelman, J.P., E. Sheen, M.P. Kavanaugh, R.A. Warren, Y. Wu, A. Lagrutta, C. Bond, and R.A. North. 1992. Calcium-activated potassium channels expressed from cloned complementary DNAs. *Neuron*. 9:209–216.

Akaike, H. 1974. A new look at the statistical model identification. *IEEE Trans. Auto. Control*. 19:716–723.

Almers, W. 1978. Gating currents and charge movements in excitable membranes. *Rev. Physiol. Biochem. Pharmacol*. 82:96–190.

Andersen, O.S. 1999. Editorial: graphic representation of the results of kinetic analyses. *J. Gen. Physiol*. 114:589–590.

Atkinson, N.S., G.A. Robertson, and B. Ganetzky. 1991. A component of calcium-activated potassium channels encoded by the *Drosophila* slo locus. *Science*. 253:551–555.

Barrett, J.N., K.L. Magleby, and B.S. Pallotta. 1982. Properties of single calcium-activated potassium channels in cultured rat muscle. *J. Physiol*. 331:211–230.

Bello, R.A., and K.L. Magleby. 1998. Time-irreversible subconductance gating coupled to permeation of Ba^{2+} through large-conductance Ca^{2+}-activated K^+ channels. *J. Gen. Physiol*. 111:343–362.

Bielefeldt, K., and M.B. Jackson. 1994. Phosphorylation and dephosphorylation modulate a Ca^{2+}-activated K^+ channel in rat peptidergic nerve terminals. *J. Physiol*. 475:241–254.

Brenner, R., T.J. Jeglas, A. Wickenden, Y. Liu, and R.W. Aldrich. 2000. Cloning and functional characterization of novel large conductance calcium-activated potassium channel β subunits, hKCNMB3 and hKCNMB4. *J. Biol. Chem*. 275:6453–6461.

Butler, A., S. Tsunoda, D.P. McCobb, A. Wei, and L. Salkoff. 1993. mSlo, a complex mouse gene encoding "maxi" calcium-activated potassium channels. *Science*. 261:221–224.

Changeux, J.-P., and S.J. Edelstein. 1998. Allosteric receptors after 30 years. *Neuron*. 21:959–980.

Colquhoun, D., and A.G. Hawkes. 1995a. The principles of the stochastic interpretation of ion-channel mechanisms. *In* Single-Channel Recording. B. Sakmann and E. Neher, editors. Plenum Publishing Corp., New York, NY. 397–482.

Colquhoun, D., and A.G. Hawkes. 1995b. A Q-matrix cookbook. *In* Single-Channel Recording. B. Sakmann and E. Neher, editors. Plenum Publishing Corp., New York, NY. 589–633.

Colquhoun, D., and F.J. Sigworth. 1995. Fitting and statistical analysis of single-channel records. *In* Single-Channel Recording. B. Sakmann and E. Neher, editors. Plenum Publishing Corp., New York, NY. 483–587.

Conley, E.C. 1996. The ion channel facts book II. Intracellular ligand-gated channels. Academic Press, Inc., New York, NY. 607–720.

Cox, D.H., J. Cui, and R.W. Aldrich. 1997. Allosteric gating of a large conductance Ca-activated K^+ channel. *J. Gen. Physiol*. 110: 257–281.

Crouzy, S.C., and F.J. Sigworth. 1990. Yet another approach to the dwell-time omission problem of single-channel analysis. *Biophys. J*. 58:731–743.

Cui, J., D.H. Cox, and R.W. Aldrich. 1997. Intrinsic voltage dependence and Ca^{2+} regulation of *mslo* large conductance Ca-activated K^+ channels. *J. Gen. Physiol*. 109:647–673.

Diaz, L., P. Meera, J. Amigo, E. Stefani, O. Alvarez, L. Toro, and R. Latorre. 1998. Role of the S4 segment in a voltage-dependent calcium-sensitive potassium (hSlo) channel. *J. Biol. Chem*. 273: 32430–32436.

DiChiara, T.J., and P.H. Reinhart. 1995. Distinct effects of Ca^{2+} and voltage on the activation and deactivation of cloned Ca^{2+}-activated K^+ channels. *J. Physiol*. 489:403–418.

DiChiara, T.J., and P.H. Reinhart. 1997. Redox modulation of *hslo* Ca^{2+}-activated K^+ channels. *J. Neurosci*. 17:4942–4955.

Eigen, M. 1968. New looks and outlooks on physical enzymology. *Q. Rev. Biophys*. 1:3–33.

Eisenberg, R.S. 1990. Channels as enzymes. *J. Membr. Biol*. 115:1–12.

Ferguson, W.B., O.B. McManus, and K.L. Magleby. 1993. Opening and closing transitions for BK channels often occur in two steps via sojourns through a brief lifetime subconductance state. *Biophys. J*. 65:702–714.

Fersht, A. 1985. Enzyme structure and mechanism. W.H. Freeman Co., San Francisco, CA. 263–278.

Fredkin, D.R., M. Montal, and J.A. Rice. 1985. Identification of aggregated Markovian models: application to the nicotinic acetylcholine receptor. *In* Proceedings of the Berkeley Conference in Honor of Jerzy Neyman and Jack Kiefer. L.M. LeCam, and R.A. Olshen, editors. Wadsworth Publishing Co., Belmont, CA. 269–289.

Hamill, O.P., A. Marty, E. Neher, B. Sakmann, and F.J. Sigworth. 1981. Improved patch clamp techniques for high-resolution current recording from cells and cell-free membrane patches. *Pflügers Arch*. 391:85–100.

Hodgkin, A.L., and A.F. Huxley. 1952. A quantitative description of membrane current and its application to conduction and excita-

tion in nerve. *J. Physiol.* 117:500–544.

Horn, R. 1987. Statistical methods for model discrimination: application to gating kinetics and permeation of the acetylcholine receptor channel. *Biophys. J.* 51:255–263.

Horrigan, F.T., and R.W. Aldrich. 1999. Allosteric voltage gating of potassium channels II. *mSlo* channel gating charge movement in the absence of Ca^{2+}. *J. Gen. Physiol.* 114:305–336.

Horrigan, F.T., J. Cui, and R.W. Aldrich. 1999. Allosteric voltage gating of potassium channels I. *mSlo* ionic currents in the absence of Ca^{2+}. *J. Gen. Physiol.* 114:277–304.

Islas, L.D., and F.J. Sigworth. 1999. Voltage sensitivity and gating charge in *Shaker* and *Shab* family potassium channels. *J. Gen. Physiol.* 114:723–741.

Jan, L.Y., and Y.N. Jan. 1997. Cloned potassium channels from eukaryotes and prokaryotes. *Annu. Rev. Neurosci.* 20:91–123.

Jones, E.M., M. Gray-Keller, and R. Fettiplace. 1999. The role of Ca^{2+}-activated K^+ channel spliced variants in the tonotopic organization of the turtle cochlea. *J. Physiol.* 518:653–665.

Jones, S.W. 1999. Commentary: a plausible model. *J. Gen. Physiol.* 114:271–275.

Kaczorowski, G.J., H.G. Knaus, R.J. Leonard, O.B. McManus, and M.L. Garcia. 1996. High-conductance calcium-activated potassium channels: structure, pharmacology, and function. *J. Bioenerg. Biomembr.* 28:255–267.

Kleinbaum, D.G, L.L. Kupper, and K.E. Muller. 1988. Applied regression analysis and other multivariable methods. Duxbury Press, Belmont, CA. 88–89.

Lagrutta, A., K.R.A. Shen, R.A. North, and J.P. Adelman. 1994. Functional differences among alternatively spliced variants of *slowpoke*, a *Drosophila* calcium-activated potassium channel. *J. Biol. Chem.* 269:20347–203511.

Latorre, R., C. Vergara, and C. Hidalgo. 1982. Reconstitution in planar lipid bilayers of a Ca^{2+}-dependent K^+-channel from transverse tubule membranes isolated from rabbit skeletal muscle. *Proc. Natl. Acad. Sci. USA.* 79:805–809.

Latorre, R. 1994. Molecular workings of large conductance (maxi) Ca^{2+} -activated K^+ channels. *In* Handbook of Membrane Channels: Molecular and Cellular Physiology. C. Peracchia, editor. Academic Press, Inc., New York, NY. 79–102.

Levitan, I.B. 1994. Modulation of ion channels by protein phosphorylation and dephosphorylation. *Annu. Rev. Physiol.* 56:193–212.

Liu, D.T., G.R. Tibbs, and S.A. Siegelbaum. 1996. Subunit stoichiometry of cyclic nucleotide-gated channels and effects of subunit order on channel function. *Neuron.* 16:983–990.

Magleby, K.L. 1992. Preventing artifacts and reducing errors in single-channel analysis. *Methods Enzymol.* 207:763–791.

Magleby, K.L., and B.S. Pallotta. 1983. Calcium-dependence of open and shut interval distributions from calcium-activated potassium channels in cultured rat muscle. *J. Physiol.* 344:585–604.

Magleby, K.L., and L. Song. 1992. Dependency plots suggest the kinetic structure of ion channels. *Proc. R. Soc. Lond. B Biol. Sci.* 249: 133–142.

Magleby, K.L., and D.S. Weiss. 1990. Identifying kinetic gating mechanisms for ion channels by using two-dimensional distributions of simulated dwell times. *Proc. R. Soc. Lond. B Biol. Sci.* 241: 220–228.

Marks, T.N., and S.W. Jones. 1992. Calcium currents in the A7r5 smooth muscle–derived cell line: an allosteric model for calcium channel activation and dihydropyridine agonist action. *J. Gen. Physiol.* 99:367–390.

Marty, A. 1981. Ca-dependent K channels with large unitary conductance in chromaffin cell membranes. *Nature.* 291:497–500.

McCormack, K., W.J. Joiner, and S.H. Heinemann. 1994. A characterization of the activation structural rearrangements in voltage-dependent *Shaker* K^+ channels. *Neuron.* 12:301–315.

McManus, O.B., A.L. Blatz, and K.L. Magleby. 1985. Inverse relationship of the durations of adjacent open and shut intervals for Cl and K channels. *Nature.* 317:625–628.

McManus, O.B., A.L. Blatz, and K.L. Magleby. 1987. Sampling, log binning, fitting, and plotting durations of open and shut intervals from single channels and the effects of noise. *Pflügers Arch.* 410:530–553.

McManus, O.B., L.M.H. Helms, L. Pallanck, B. Ganetzky, R. Swanson, and R.J. Leonard. 1995. Functional role of the beta subunit of high-conductance calcium-activated potassium channels. *Neuron.* 14:645–650.

McManus, O.B., and K.L. Magleby. 1988. Kinetic states and modes of single large-conductance calcium-activated potassium channels in cultured rat skeletal muscle. *J. Physiol.* 402:79–120.

McManus, O.B., and K.L. Magleby. 1989. Kinetic time constants independent of previous single-channel activity suggest Markov gating for a large-conductance Ca-activated K channel. *J. Gen. Physiol.* 94:1037–1070.

McManus, O.B., and K.L. Magleby. 1991. Accounting for the Ca^{2+}-dependent kinetics of single large-conductance Ca^{2+}-activated K^+ channels in rat skeletal muscle. *J. Physiol.* 443:739–777.

Meera, P., M. Wallner, Z. Jiang, and L. Toro. 1996. A calcium switch for the functional coupling between α (*hslo*) and β subunits (K_v, Cab) of maxi K channels. *FEBS Lett.* 382:84–88.

Methfessel, C., and G. Boheim. 1982. The gating of single calcium-dependent potassium channels is described by an activation/blockade mechanism. *Biophys. Struct. Mech.* 9:35–60.

Moczydlowski, E., and R. Latorre. 1983. Gating kinetics of Ca^{2+}-activated K^+ channels from rat muscle incorporated into planar lipid bilayers: evidence for two voltage-dependent Ca^{2+} binding reactions. *J. Gen. Physiol.* 82:511–542.

Monod, J., J. Wyman, and J.-P. Changeux. 1965. On the nature of allosteric transitions: a plausible model. *J. Mol. Biol.* 12:88–118.

Nimigean, C.M., and K.L. Magleby. 1999. The β subunit increases the Ca^{2+}-sensitivity of large conductance Ca^{2+}-activated channels by retaining the gating in the bursting states. *J. Gen. Physiol.* 113: 425–439.

Nimigean, C.M., B.L. Moss, and K.L. Magleby. 1999. Single-channel gating kinetics of BK channels in 0 μM Ca^{2+} are inconsistent with gating models based on the Monod-Wyman-Changeux (MWC) model for tetrameric allosteric proteins. *Soc. Neurosci. Abstr.* 25: 985.

Nimigean, C.M., and K.L. Magleby. 2000. Gating in the absence of Ca^{2+}_i reveals Ca^{2+}_i-independent coupling of the β_1 subunit to large conductance Ca^{2+}-activated K^+ (BK) channels: increased Ca^{2+} sensitivity from a Ca^{2+}-independent mechanism. *J. Gen. Physiol.* 115:719–734.

Pallanck, L., and B. Ganetzky. 1994. Cloning and characterization of human and mouse homologs of the *Drosophila* calcium-activated potassium channel gene, slowpoke. *Hum. Mol. Genet.* 3:1239–1243.

Pallotta, B.S., K.L. Magleby, and J.N. Barrett. 1981. Single channel recordings of Ca^{2+}-activated K^+ curtrents in rat muscle cell culture. *Nature.* 293:471–474.

Pallotta, B.S. 1985. *N*-Bromoacetamide removes a calcium-dependent component of channel opening from calcium-activated potassium channels in rat skeletal muscle. *J. Gen. Physiol.* 86:601–611.

Reinhart, P.H., S. Chung, B.L. Martin, D.L. Brautigan, and I.B. Levitan. 1991. Modulation of calcium-activated potassium channels from rat brain by protein kinase A and phosphatase 2A. *J. Neurosci.* 11:1627–1635.

Ríos, E., M. Karhanek, J. Ma, and A. Gonzalez. 1993. An allosteric model of the molecular interactions of excitation–contraction coupling in skeletal muscle. *J. Gen. Physiol.* 102:449–481.

Rothberg, B.S., R.A. Bello, L. Song, and K.L. Magleby. 1996. High

Ca^{2+} concentrations induce a low activity mode and reveal Ca^{2+}-independent long shut intervals in BK channels from rat muscle. *J. Physiol.* 493:673–689.

Rothberg, B.S., and K.L. Magleby. 1996. Gating of BK channels can be independent of calcium or voltage. *Soc. Neurosci. Abstr.* 22: 1443.

Rothberg, B.S., and K.L. Magleby. 1998. Kinetic structure of large-conductance Ca^{2+}-activated K^+ channels suggests that the gating includes transitions through intermediate or secondary states: a mechanism for flickers. *J. Gen. Physiol.* 111:751–780.

Rothberg, B.S., and K.L. Magleby. 1999. Gating kinetics of single-large-conductance Ca^{2+}-activated K^+ channels in high Ca^{2+} suggest a two-tiered allosteric gating mechanism. *J. Gen. Physiol.* 114: 95–124.

Roux, M.J., R. Olcese, L. Toro, F. Bezanilla, and E. Stefani. 1998. Fast inactivation in *Shaker* K^+ channels. Properties of ionic and gating currents. *J. Gen. Physiol.* 111:625–638.

Schoppa, N.E., K. McCormack, M.A. Tanouye, and F.J. Sigworth. 1992. The size of gating charge in wild-type and mutant *Shaker* potassium channels. *Science.* 255:1712–1715.

Schoppa, N.E., and F.J. Sigworth. 1998. Activation of *Shaker* potassium channels. III. An activation gating model for wild-type and V2 mutant channels. *J. Gen. Physiol.* 111:313–342.

Schreiber, M., and L. Salkoff. 1997. A novel calcium-sensing domain in the BK channel. *Biophys. J.* 73:1355–1363.

Schreiber, M., A. Yuan, and L. Salkoff. 1999. Transplantable sites confer calcium sensitivity to BK channels. *Nat. Neurosci.* 2:416–421.

Shen, K.-Z., A. Lagrutta, N.W. Davies, N.B. Standen, J.P. Adelman, and R.A. North. 1994. Tetraethylammonium block of *slowpoke* calcium-activated potassium channels expressed in *Xenopus* oocytes: evidence for tetrameric channel formation. *Pflügers Arch.* 426: 440–445.

Sigg, D., and F. Bezanilla. 1997. Total charge movement per channel: the relation between gating charge displacement and the voltage-sensitivity of activation. *J. Gen. Physiol.* 109:27–39.

Sigg, D., J. Qian, and F. Bezanilla. 1999. Kramers' diffusion theory applied to gating kinetics of voltage-dependent ion channels. *Biophys. J.* 76:782–803.

Sigworth, F.J. 1994. Voltage gating of ion channels. *Q. Rev. Biophys.* 27:1–40.

Smith, M.A., and M.L.J. Ashford. 1998. Mode switching characterizes the activity of large conductance potassium channels recorded from rat cortical fused nerve terminals. *J. Physiol.* 513: 733–747.

Song, L., and K.L. Magleby. 1994. Testing for microscopic reversibility in the gating of maxi K^+ channels using two-dimensional dwell-time distributions. *Biophys. J.* 67:91–104.

Stefani, E., M. Ottolia, F. Noceti, R. Olcese, M. Wallner, R. Latorre, and L. Toro. 1997. Voltage-controlled gating in a large conductance Ca^{2+}-sensitive K^+ channel (hslo). *Proc. Natl. Acad. Sci. USA.* 94:5427–5431.

Stevens, C.F. 1978. Interactions between intrinsic membrane protein and electric field: an approach to studying nerve excitability. *Biophys. J.* 22:295–306.

Talukder, G., and R.W. Aldrich. 2000. Complex voltage-dependent behavior of single unliganded calcium-sensitive potassium channels. *Biophys. J.* 78:761–772.

Tanaka, Y., P. Meera, M. Song, H.-G. Knaus, and L. Toro. 1997. Molecular constituents of maxi Kca channels in human coronary smooth muscle: predominant $\alpha + \beta$ subunit complexes. *J. Physiol.* 502:545–557.

Thuringer, D., and I. Findlay. 1997. Contrasting effects of intracellular redox couples on the regulation of maxi-K channels in isolated myocytes from rabbit pulmonary artery. *J. Physiol.* 500:583–592.

Toro, L., M. Wallner, P. Meera, and Y. Tanaka. 1998. Maxi-K_{Ca}, a unique member of the voltage-gated K channel superfamily. *News Physiol. Sci.* 13:112–117.

Tseng-Crank, J., C.D. Foster, J.D. Krause, R. Mertz, N. Godinot, T.J. DiChiara, and P.H. Reinhart. 1994. Cloning, expression, and distribution of functionally distinct Ca^{2+}-activated K^+ channel isoforms from human brain. *Neuron.* 13:1315–1330.

Wallner, M., P. Meera, and L. Toro. 1999. Molecular basis of fast inactivation in voltage and Ca^{2+}-activated K^+ channels: a transmembrane beta-subunit homolog. *Proc. Natl. Acad. Sci. USA.* 96: 4137–4142

Wei, A., C. Solaro, C. Lingle, and L. Salkoff. 1994. Calcium sensitivity of BK-type K_{Ca} channels determined by a separable domain. *Neuron.* 13:671–680.

Weiss, D.S., and K.L. Magleby. 1992. Voltage-dependent gating mechanism for single fast chloride channels from rat skeletal muscle. *J. Physiol.* 453:279–306.

Wong, B.S., H. Lecar, and M. Adler. 1982. Single calcium-dependent potassium channels in clonal anterior pituitary cells. *Biophys. J.* 39:313–317.

Wu, Y.-C., J.J. Art, M.B. Goodman, and R. Fettiplace. 1995. A kinetic description of the calcium-activated potassium channel and its application to electrical tuning of hair cells. *Prog. Biophys. Mol. Biol.* 63:131–158.

Xia, X.M., J.P. Ding, and C.J. Lingle. 1999. Molecular basis for the inactivation of Ca^{2+}- and voltage-dependent BK channels in adrenal chromaffin cells and rat insulinoma tumor cells. *J. Neurosci.* 19:5255–5264.

Zagotta, W.N., T. Hoshi, and R.W. Aldrich. 1994. *Shaker* potassium channel gating. III: evaluation of kinetic models for activation. *J. Gen. Physiol.* 103:321–362.

Zheng, J., and F.J. Sigworth. 1998. Intermediate conductances during deactivation of heteromultimeric *Shaker* potassium channels. *J. Gen. Physiol.* 112:457–474.